The merger history, AGN and dwarf galaxies of Hickson Compact Group 59

I. S. Konstantopoulos[1], S. C. Gallagher[2], K. Fedotov[2,3], P. R. Durrell[4], P. Tzanavaris[5,6,7],
A. R. Hill[2], A. I. Zabludoff[8], M. L. Maier[9], D. M. Elmegreen[10], J. C. Charlton[1],
K. E. Johnson[11,12], W. N. Brandt[1], L. M. Walker[11], M. Eracleous[1], A. Maybhate[13],
C. Gronwall[1], J. English[14], A. E. Hornschemeier[5], J. S. Mulchaey[15]

ABSTRACT

Compact group galaxies often appear unaffected by their unusually dense environment. Closer examination can, however, reveal the subtle, cumulative effects of multiple galaxy interactions. Hickson Compact Group (HCG) 59 is an excellent example of this situation. We present a photometric study of this group in the optical (*HST*), infrared (*Spitzer*) and X-ray (*Chandra*) regimes aimed at characterizing the star formation and nuclear activity in its constituent galaxies and intra-group medium. We associate five dwarf galaxies with the group and update the velocity dispersion, leading to an increase in the dynamical mass of the group of up to a factor of 10 (to 2.8×10^{13} M$_\odot$), and a subsequent revision of its evolutionary stage. Star formation is proceeding at a level consistent with the morphological types of the four main galaxies, of which two are star-forming and the other two quiescent. Unlike in some other compact groups, star-forming complexes across HCG 59 closely follow mass-radius scaling relations typical of nearby galaxies. In contrast, the ancient globular cluster populations in galaxies HCG 59A and B show intriguing irregularities, and two extragalactic H II regions are found just west of B. We age-date a faint stellar stream in the intra-group medium at ~ 1 Gyr to examine recent interactions. We detect a likely low-luminosity AGN in HCG 59A by its $\sim 10^{40}$ erg s^{-1} X-ray emission; the active nucleus rather than star formation can account for the UV+IR SED. We discuss the implications of our findings in the context of galaxy evolution in dense environments.

Subject headings: galaxies: clusters: individual (HCG 59) — galaxies: star clusters — galaxies: evolution — galaxies: interactions — galaxies: active — galaxies: dwarf — galaxies: fundamental parameters

[1]Department of Astronomy & Astrophysics, The Pennsylvania State University, University Park, PA 16802; iraklis@astro.psu.edu

[2]Department of Physics & Astronomy, The University of Western Ontario, London, ON N6A 3K7, Canada

[3]Herzberg Institute of Astrophysics, Victoria, BC V9E 2E7, Canada

[4]Department of Physics & Astronomy, Youngstown State University, Youngstown, OH 44555

[5]Laboratory for X-ray Astrophysics, NASA Goddard Space Flight Center, Greenbelt, MD 20771

[6]Department of Physics and Astronomy, The Johns Hopkins University, Baltimore, MD 21218

[7]NASA Post-doctoral Program Fellow

[8]Steward Observatory, University of Arizona, Tucson, AZ 85721

[9]Gemini Observatory, Casilla 603, Colina el Pino S/N,

1. Introduction

Compact galaxy groups populate the high density tail of the galaxy number density distribution.

La Serena, Chile

[10]Department of Physics & Astronomy, Vassar College, Poughkeepsie, NY 12604

[11]Department of Astronomy, University of Virginia, Charlottesville, VA 22904

[12]National Radio Astronomy Observatory, Charlottesville, VA 22903

[13]Space Telescope Science Institute, Baltimore, MD 21218

[14]University of Manitoba, Winnipeg, MN, Canada

[15]Carnegie Observatories, Pasadena, CA 91101

1

The systems catalogued by Hickson (1982, Hickson Compact Groups, or HCGs) exhibit some features, such as dynamical and evolutionary states, elliptical fractions and X-ray properties of the intra-group medium (IGM) similar to galaxy clusters, their massive, more populous counterparts. In contrast to the well-studied cluster galaxies, however, the specific effects of the compact group environment on the evolution of its galaxies are not yet clear.

HCGs are defined through criteria of isolation and surface brightness[1] that give rise to self-gravitating, dense groupings of a few (typically four) main members. Because of their masses, these galaxies orbit around the group barycenter rather sluggishly, with velocity dispersions on the order of $\sigma_{\mathrm{CG}} \sim 250$ km s^{-1} (Tago et al. 2008; Cox 2000), *cf.* galaxy cluster dispersions of $\sigma_{\mathrm{cluster}} \sim 750$ km s^{-1} (Binggeli et al. 1987; The & White 1986; Cox 2000). This trait makes HCGs valuable laboratories for galaxy evolution: the low velocity dispersions force some galaxies into strong, prolonged interactions while others appear undisturbed but are apparently undergoing enhanced secular evolution. That is to say, this latter population is affected by gravitational interplay with their neighbors, but evolve more subtly, without obvious, strong interactions (Konstantopoulos et al. 2010).

Relating the various observational characteristics of compact groups to those of clusters is important for understanding whether they constitute their own class, or if they are simply mini-clusters. Perhaps more appropriately, structures like compact groups may be considered plausible building blocks of clusters at higher z (e. g. Fujita & Goto 2004; Rudick et al. 2006). Revealing past investigations of HCGs as a class have focussed on gas content. Their members are typically deficient in H I gas when compared to galaxies of similar morphological types and masses (e. g. the sample of isolated galaxies in Haynes & Giovanelli 1984). Verdes-Montenegro et al. (2001) proposed an evolutionary sequence based on mapping the spatial distribution of H I across a large sample of HCGs. Johnson et al. (2007, hereafter J07) added

to this investigation by quantifying the gas richness of twelve groups with the relation of H I-to-dynamical mass, $\log(M_{\mathrm{H\,I}})/\log(M_{\mathrm{dyn}})$. This gave rise to the hypothesis of an alternate, two-pronged evolutionary diagram for HCGs, which we explored in Konstantopoulos et al. (2010). In one path, the galaxies have strong interactions before exhausting their cold gas reservoirs for star formation, in the other, gas is processed by star formation within individual galaxies prior to late-stage dry mergers.

Furthermore, the mid-IR colors of HCG galaxies show an interesting bimodal distribution that distinguishes star-forming from quiescent systems. Walker et al. (2010) interpret this statistically significant gap as evidence for accelerated galaxy evolution in the compact group environment. Their similar mid-IR color distributions relate HCGs to the infall regions of clusters and set them apart from any other galaxy sample compared, interacting or quiescent. This theme was expanded by Tzanavaris et al. (2010) who found this gap apparent also in the distribution of specific star formation rates for HCG galaxies. These observations together point to compact groups as local examples of the plausible building blocks of clusters in the early universe.

In addition, HCGs, which are isolated by selection, could potentially help explain the evolutionary history of some field ellipticals. For example, Rubin et al. (1990) originally proposed (see also Gallagher et al. 2008) that HCG 31 will evolve into a single, field elliptical through a wet merger (one where gas is still available during the interaction). 'Fossil groups', the probable ultimate fate of isolated groupings, were examined by Jones et al. (2003), who defined a criterion of diffuse X-ray emission in excess of $0.5 \times 10^{42} h_{70}^{-2}$ erg s^{-1} for such a classification. This arises from the processing of a group's IGM during a merger (or series of mergers), but the low total mass of most local compact groups suggests their potential well lacks the depth required to heat the IGM to X-ray detectable levels (Mulchaey & Zabludoff 1998). Using multiple mergers as a vehicle toward a fossil group end-state maps one path of galaxy evolution from the 'blue cloud' of star-forming disk galaxies to the 'red sequence' of quiescent bulge-dominated galaxies (Bell et al. 2004).

Fossil group formation may provide an analogy

---

[1] $\theta_N \geq 3\,\theta_G$, *i. e.* a circular area defined by three galaxy-mean-radii about the group is devoid of galaxies of comparable brightness. A group surface brightness of $\mu <$ 26.0 mag defines galaxy density.

to cluster centers or sub-clumps where the buildup of cD galaxies occurs. If this turns out to be valid, the study of compact groups could also help illuminate morphological transformations in the innermost cores of clusters. Exploring these different scenarios may prove fruitful for our understanding of galaxy evolution and the buildup of stellar mass in the universe. Making meaningful progress in this area requires detailed multi-wavelength studies in order to map the range of physical processes affecting galaxies that are found in these environments, determine their histories, and project their evolution.

A consistent treatment of a large sample of HCGs is therefore in order. In this work we continue the series of Gallagher et al. (2010) and Konstantopoulos et al. (2010) and provide a comprehensive, multi-wavelength study of HCG 59. We will look at the current state of the group through its star formation and nuclear activity; investigate its past through the star cluster populations; try to unravel the history of mergers in the group; examine its dwarf galaxy system; and place it in the context of HCGs in general.

The core of HCG 59 consists of four giant galaxies, a typical number for HCGs in general. The group lies at a distance of 60 Mpc, based on a recession velocity of $v_R = 4047$ km s^{-1} (Hickson et al. 1992, corrected to the reference frame defined by the 3K Microwave Background) and $H_0 = 73$ km s^{-1} Mpc^{-1}. Three of the galaxies, A (type Sa), B (E0), and C (Sc), have seemingly undisturbed morphologies, and the fourth (D, Im) is an unusually large irregular with a normal, peaked light profile. The total stellar mass of the group is $M^*_{\rm TOT} = 3.14 \times 10^{10}$ M$_\odot$ (from the 2MASS K_s-band luminosities; Tzanavaris et al. 2010), while the H I mass of $M_{\rm H\,I} = 3.09 \times 10^9$ M$_\odot$ is comparable to the value expected for the morphological types and stellar masses of the member galaxies, according to Verdes-Montenegro et al. (2001). This is therefore a somewhat gas-rich compact group, given that HCGs typically contain only about a third of the H I expected. On the other hand, the J07 scheme classifies the H I content of the galaxy group as a Type II, $i.\,e.$ intermediate in gas content, according to its ratio of gas-to-dynamical mass of $\log(M_{\rm H\,I})/\log(M_{\rm dyn}) = 0.81 \pm 0.05$. These classifications are based on different criteria and the disparity can thus be rec-

onciled. Table 1 summarizes some of the general characteristics of the four galaxies, while Table ?? presents some derived and literature values of the mass content and nuclear identifications in the four galaxies.

This paper is organized in the following way: Section 2 presents the optical, IR, and X-ray datasets used throughout this work. Section 3 provides a full account of the young and old star cluster populations, which we use as our prime diagnostics of current star formation and ancient interactions. In Section 4 we discuss the main findings of this work. Finally, in Section 5 we summarize the work presented and offer ties to previous and future work in this series.

2. Observations

2.1. *HST* optical imaging

The analysis presented in this paper is based largely on *HST*-ACS/WFC multi-band data. Images were taken in the *F435W, F606W* and *F814W* bands in two pointings to cover all known giant group members. We will refer to these filters as B_{435}, V_{606}, I_{814} (and the set as BVI) to denote the closest matches in the Johnson photometric system. The notation does not, however, imply a conversion between the two systems. The observations were executed on 2007 February 24, as part of GO program 10787 (PI: Jane Charlton). The exposure times were 1710, 1230 and 1065 seconds in the BVI bands respectively. Three equal sub-exposures were taken with each filter with a three-point dither pattern (sub-pixel dithering). Images were reduced 'on the fly' to produce combined, geometrically corrected, cosmic-ray cleaned images. For the analysis of point sources, we used the standard *HST* pipeline products with a nominal pixel scale of 0$.\!''$05 per pixel. For analysis of the extended sources, we ran `MultiDrizzle` (Fruchter & Sosey 2009) with the pixel scale set to 0$.\!''$03 per pixel to improve the spatial resolution. The absolute image astrometry was checked with the world coordinate system of the Two Micron All-Sky Survey catalog (2MASS; Skrutskie et al. 2006) by identifying four unsaturated point sources in common; the average offset was $\sim 0.01''$ in RA and Dec. The four main galaxy I_{814}-band light profiles were fit with Sérsic profiles using GALFIT (Sérsic 1968; Peng et al. 2010a);

Table 1: Basic information on HCG 59 main members

Identifier	Coordinates[a] (J2000)	Type H89[c]	m (mag)	v_R ($\mathrm{km\,s^{-1}}$)	References[b]
A: IC 0737	11:48:27.55 +12:43:38.7	Sa	14.82 (B)	4109	[1], [2], [3]
B: IC 0736	11:48:20.08 +12:42:59.5	E0[d]	15.60 (B)	4004	[4], [2], [5]
C: KUG 1145+129	11:48:32.44 +12:42:19.5	Sc	15.90 (g)	4394	[4], [2]
D: KUG 1145+130	11:48:30.64 +12:43:47.8	Im	16.00 (g)	3635	[4], [2]

.

[a]Coordinates are the centroids from fitting the *HST* I_{814}-band images of each galaxy with Sérsic profiles. See § 2.1 for more details.

[b][1]: Evans et al. (2010); [2]: de Vaucouleurs et al. (1991); [3]: Hickson et al. (1992); [4]: York et al. (2000); [5]: Falco et al. (1999).

[c]Hickson et al. (1989)

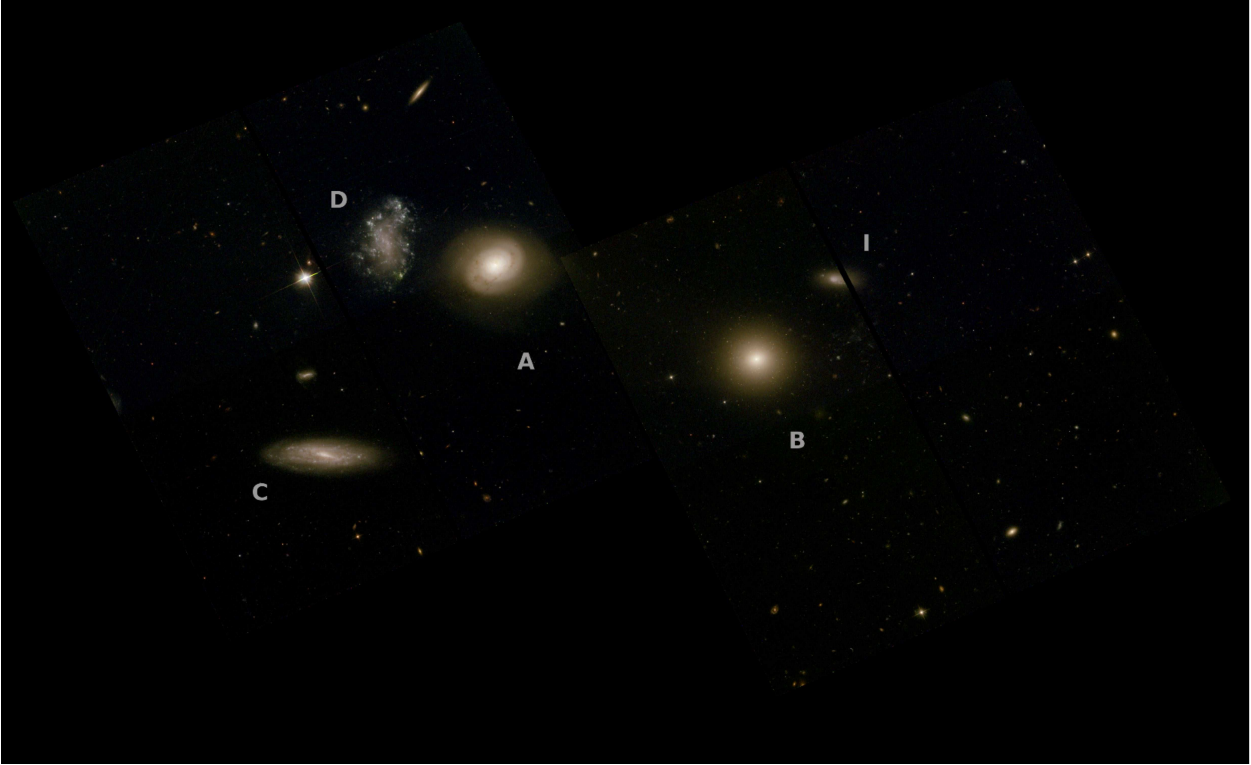[d]The RC3 designation for 59B is' S0?', and so there is some uncertainty as to its classification.

Fig. 1.— *HST BVI* color-composite imaging of HCG 59. The red colors of galaxies A and B imply little star formation, while C and D show some signatures of nebular emission in green. Also visible is the newly catalogued dwarf galaxy I (Section 4.1).

Table 2: Masses and star formation rates of HCG 59 galaxies

ID	M_*[a]	M_{H_2}[b]	SFR[c]	sSFR[d]	Nucleus [e]
	$(\times 10^9$ M$_\odot)$		(M$_\odot$ yr^{-1})	$(\times 10^{-11}$ yr$^{-1})$	
A	17.40	10.2	4.99 ± 0.67[f]	28.66	C/AGN
B	8.29	< 8.8	0.02 ± 0.01	0.19	C
C	3.03	< 7.2	0.16 ± 0.03	5.15	H II
D	2.67	< 6.6	0.48 ± 0.04	18.15	H II

[a,c,d]Stellar masses, star formation rates (SFR) and specific SFRs (sSFR) are drawn from Tzanavaris et al. (2010). The published stellar masses were off by a factor of 7.4; these values have been corrected for this error.

[b]From the CO observations of Verdes-Montenegro et al. (1998)

[e]From Martínez et al. (2010); 'C' stands for 'composite', *i.e.* one that falls at the H II/AGN overlap region, as defined in Kewley et al. (2006); see Sections 4.4, 4.5 for discussion on these designations.

[f]This value is heavily affected by the AGN in galaxy A, as will be elaborated in Section 2.6.

the best-fitting centroid positions are given in Table 1.

We used the images, presented in Figure 1, to characterize the optical morphology of the galaxies, and to detect and photometer star clusters and cluster complexes. All reported magnitudes are in the Vega magnitude system. In Section 3, we present the analysis of these two scales (clusters and complexes) of the star formation hierarchy and also distinguish between young massive clusters (YMCs) and globular clusters (GCs).

2.2. Optical point source photometry

We follow the same rationale applied in our previous work (Gallagher et al. 2010; Konstantopoulos et al. 2010) and use star clusters to infer the star formation activity and history in each of the HCG 59 galaxies. At the adopted distance to HCG 59 of 60 Mpc, we expect some contamination by supergiant stars, which can have absolute V-band magnitudes as bright as -8.5 (Efremov et al. 1986). At this distance, one ACS pixel measures ~ 13 pc, (*cf.* the average star cluster radius of ~ 4 pc; e.g. Scheepmaker et al. 2007), meaning that clusters are at most marginally resolved and can be considered point sources for the purposes of selection and photometry. We select clusters using the method described in Gallagher et al. (2010); in brief, we perform the initial selection on median-divided images, require selection in all three bands, and filter the resulting catalog using point spread function (PSF) photometry. Our PSF filtering applied the following criteria from the output of the `ALLSTAR`

routine in IRAF[2]: χ values below 3.0; a sharpness in the range $[-2.0, 2.0]$; and a photometric error less than 0.3 mag. Aperture corrections are first measured between 3 and 10 pixels and then added to the Sirianni et al. (2005) corrections to infinity. Finally, foreground (Galactic) extinction with $E(B - V) = 0.037$ is accounted for using the standard Galactic extinction law (a correction of $A_V \sim 0.12$ mag; Schlegel et al. 1998).

In order to fortify the selection against stars, we apply a conservative absolute magnitude cut at $M_V < -9$ mag, which produces the high-confidence sample. We do, however, define a larger sample by relaxing the magnitude cut and applying stricter PSF-fitting criteria to detect globular clusters, which are expected to be fainter and point-like. In order to minimize contamination from marginally resolved sources such as compact background galaxies, we follow Rejkuba et al. (2005) and apply hyperbolic filters (starting narrow for bright sources and widening for fainter sources) with a maximum cut-off at the above mentioned criteria of magnitude error, χ and sharpness. We will refer to this as the extended sample.

The application of these criteria assigns 240 bright star cluster candidates (SCCs) to the high-confidence sample and 948 to the extended sample. Specifically, the numbers of detected SSCs (ex-

tended sample numbers in parentheses) in galaxies A through D are 7 (29), 77 (213), 13 (63) and 65 (217), with a further 78 (426) objects coincident with what would be the intra-group medium. We will provide a full analysis of these cluster populations in Section 3.1.

In order to test the completeness of the final list of SCCs, we used `ADDSTAR` to add 3000 artificial stars to the image (over the entire field, including the galaxies) in the apparent magnitude range 24–28, $i.\,e.$ absolute magnitudes of $(-9.89, -5.89)$. Because the final catalogue only contains sources detected in all three filters, we include this effect by calculating completeness fractions based only on artificial stars detected in all three bands (e. g. Da Rocha et al. 2002). The limiting magnitudes for the 90% and 50% recovery rates are (26.56, 27.25), (26.51, 27.19) and (26.47, 27.15) in the B_{435}, V_{606} and I_{814} bands respectively (after photometric corrections are applied). For the distance modulus used of 33.89 mag, $m = 26.5$ mag corresponds to $M \simeq -7.4$ mag.

Our assessment of the state of star formation in HCG 59 is not limited to star clusters. Star cluster complexes represent a larger scale of star formation, as the optically blended concentrations of gas, stars, and dust that make up small starforming regions, and likely include groups of clusters. In contrast to star clusters, these can be resolved to even greater distances than studied here, as the fractal distribution of gas about a galaxy gives rise to such structures at all scales (e. g. as demonstrated for M33 by Bastian et al. 2007).

2.3. Globular Cluster Candidate Selection

Globular clusters are also selected from the HST images. Since the process is tuned to the color distributions found in HCG 59, we provide a full account below. As contamination from supergiants is not a problem for objects with GC-like colors, we adopt a fainter magnitude limit to select old GC candidates than we used for SCCs. We have chosen a cutoff at $V_{606} = 26$, which corresponds to $M_V \sim -7.7$ at our adopted distance modulus for HCG 59, or slightly more luminous than the expected peak in the globular cluster luminosity function (GCLF) at $M_V \sim -7.4$ (e.g. Ashman & Zepf 1998; Harris 2001). The majority of GC candidates brighter than this limit lie above the 90% photometric completeness level in

all 3 filters. Assuming a Gaussian GC luminosity function with a peak at $M_V = -7.4 \pm 0.2$ and a dispersion $\sigma = 1.2 \pm 0.2$, our faint-end cutoff then samples $39 \pm 8\%$ of the entire GCLF.

We have selected GC candidates (GCCs) according to the color-space distribution of Milky Way GCs. We de-reddened the colors of globular clusters from the Harris (1996) catalog by their listed $E(B - V)$ values, and then defined a parallelogram based on the intrinsic $(B - V) - (V - I)$ color distribution of the MW GCs. This parallelogram was then converted to the ACS filters using the 'synthetic' transformations in Sirianni et al. (2005). The color selection region adopted here is 0.10 mag wider in $(V - I)$ than that used in the analysis of HCG 7 (Konstantopoulos et al. 2010), but still does not exceed the boundaries of the Harris (1996) MW GCs. To quantify, 95 of 97 MW GCs from the Harris (1996) catalog (those with BVI information) lie within this box. All point sources in the HCG 59 fields with 1σ error bars that overlap our color selection region are considered GC candidates, and are plotted in Figure 2.

Due to the close (projected) proximity of the galaxies in the group, it is likely that the halo GCs in each system will appear superposed. In an attempt to quantify the GCCs in each galaxy, we use the relationship between the galactic mass and the radial extent of the GC systems in galaxies of Rhode et al. (2007). To compute the expected size of each halo, we have adopted the mass-to-light conversions in that work, although we stress the general conclusions we reach are not dependent on the detailed size of any given halo. As the predicted masses of all of the group galaxies are just below the lowest mass galaxies in the Rhode et al. (2007) sample, we adopted a radial extent of 15 kpc (or $56''$ at the assumed distance to HCG 59) for each of galaxies A, B and C. Galaxy D is a lower luminosity system, and as seen in Figure 2, GCCs in this object already lie within the projected halo of GCCs in galaxy A. Discussion of the individual GC systems in each group galaxy follows in Section 3.3.

2.4. Background and Foreground Contamination

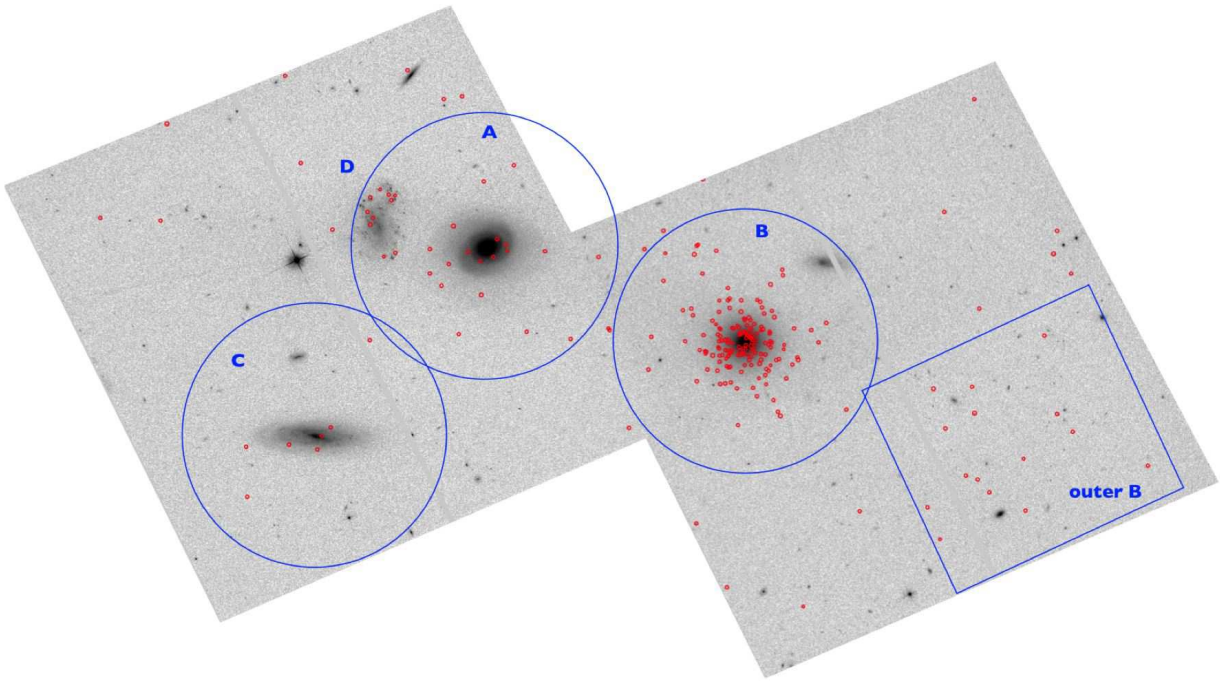Contamination in our color-selected sample of GC candidates is expected from a variety of

Fig. 2.— Positions of detected globular cluster candidates, marked on *HST* I_{814} imaging. We have also marked the expected GC haloes with blue boundaries. 'Outer B' refers to the location of a possible excess of GCs, discussed in the text. This is symmetric to the 'A-B bridge' (with respect to B; see Fig. 4) and could be a tidally induced redistribution of the GC population (see Sections 3.3 and 4.4).

sources, including foreground Milky Way halo stars, reddened young clusters, and unresolved background galaxies. With the small number of GC candidates present in some of the HCG 59 galaxies (discussed below), contamination can be significant.

Predictions from Milky Way star count models (the Besançon model of Robin et al. 2003) suggest that only 3–4 foreground Milky Way stars will appear in the magnitude and color ranges for expected GCs in each of our ACS fields. Determining the contamination from younger, reddened clusters is more difficult, particularly in the central regions of the late-type galaxies C and D, where such objects could be present. Unresolved background galaxies are not likely contributing in any significant way to the numbers of objects in our fields; analyses of the background objects (with GC-like colors) in HCG 7 (Konstantopoulos et al. 2010) showed that the predicted foreground Milky Way star counts were similar to the observed putative background contamination, leaving little room for background galaxies to contribute significantly.

We also consider the Pirzkal et al. (2005) analysis of stars in the Hubble Ultra-Deep Field (HUDF). Within the range of colors shown in Figure 8, they found the main contaminant of 'void sky' to be M-stars, however, with a V_{606}-I_{814} of ~ 2.0, they are too red to be considered in our analysis. All Main Sequence stars detected in the HUDF are too bright to be mistaken for star clusters by our detection algorithm. In fact, the only class of stellar object that can be found in the color-space occupied by our cluster candidates is white dwarfs, which Pirzkal et al. find to have a density of $1.1 \pm 0.3 \times 10^{-2}$ pc^{-3}. The maximum Galactic volume covered by our two pointings is a cube of ~ 8000 px on a side, or ~ 0.24 pc^{-3}, assuming a scale height of 400 pc (the maximum height quoted by Pirzkal et al.). Such a volume might be expected to host $\sim 2.6 \times 10^{-3}$ white dwarfs. Therefore, we consider this potential source of contamination to be negligible.

The dominant source of contamination to our GCC sample will actually be stars from the Sagittarius dwarf galaxy. Our ACS fields (at $l \sim 254°$, $b \sim +69°$) are superposed on a rather dense part of the tidally induced (and bifurcated) leading arm (stream 'A' from Belokurov et al. 2006) of Sgr (e.g., Majewski et al. 2003; Belokurov et al.

2006; Newberg et al. 2007; Yanny et al. 2009); the presence of such streams is not accounted for in traditional Milky Way star count models. To investigate the impact of Sgr Stream stellar populations, in Figure 3 we have overlaid 12 Gyr isochrones of Marigo et al. (2008) with a range of metallicities expected for the Sgr leading arm, [M/H] $\sim -1 \pm 0.5$ (e.g. Chou et al. 2007; Yanny et al. 2009), at distances between 26 and 36 kpc onto color-magnitude diagrams of the point sources in both of our ACS fields (assuming $d \sim 31$ kpc, with a spread of ± 5 kpc; Newberg et al. 2007; Niederste-Ostholt et al. 2010; Correnti et al. 2010). From this, we see that stars just below the Sgr Stream main sequence turnoff do have colors and magnitudes similar to that of the brighter ($V_{606} < 25$) GC candidates in our study, making some contamination likely.

To estimate the *total* contamination in our GCC sample, we assume those GC candidates that lie far outside the GC system halos (as shown in Figure 2) are instead contaminating sources. The one exception to this is a region (called 'outer B' in Figure 2) that lies outside the GC system of galaxy B, opposite to the direction of galaxy A. We will return to this feature below. There are a total of 18 objects in 8.4 arcmin^2, or a background surface density $\Sigma_{back} = 2.3 \pm 0.5$ arcmin^{-2}. This is much higher than the predicted surface density of MW halo stars from the Besançon model ($\Sigma_{MW} \sim 0.4$ arcmin^{-2}), indicating that Sgr leading arm stars are the dominant foreground source of contamination in our sample.

Of course, for the above analysis we are making the assumption that these contaminating objects are not *bona-fide* 'intra-group' GCs that lie far outside the main galaxies of the group. To test this, we compare the V_{606} luminosity function for the background source sample with the luminosity function of the large GC candidate population surrounding galaxy B. We show this in the right panel of Figure 3. The extrahalo luminosity function does not show a sharp rise with increasing magnitude as expected of a GC luminosity function and exhibited by the GCCs in galaxy B. Although a definitive comparison is not possible with so few objects in the IGM area, this is consistent with these IGM objects being contaminants and not a part of a diffuse population of intragroup GCs. Thus we adopt the surface density above
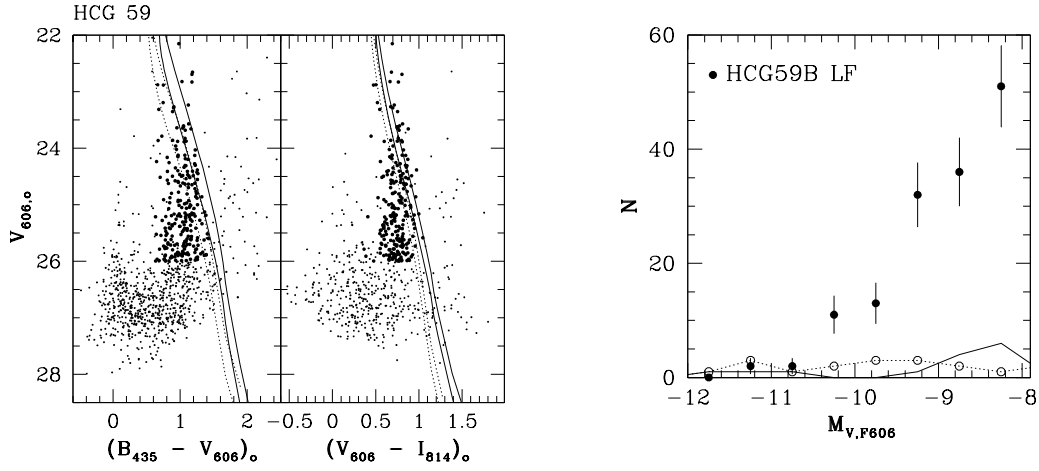
Fig. 3.— Diagnostic diagrams related to the GC population. On the **left** we show color-magnitude diagrams of all detected GCCs. The solid and dashed lines show Marigo et al. (2008) evolutionary tracks for 12 Gyr-old main sequence stars, with $Z = -0.6$ and -1.3 respectively. The lines are double to bracket the distances appropriate for the Sagittarius dwarf, with its leading spiral arm superposed along this line of sight. Their distribution in the CMD dispels our worries of significant contamination. The **right** panel shows the luminosity function of globular clusters candidates (filled circles) in galaxy B and sources considered 'background' (open circles and dashed lines). The clear discrepancy supports the quality of our GC selection. The LF of 'outer B' sources is designated with a solid line.

as that of the 'background' in the analyses that follow.

2.5. Las Campanas wide-field imaging: low surface brightness light and dwarf galaxies

We extend the coverage of the *HST* observations through wide-field imaging with the Las Campanas Observatory (LCO) 2.5-meter telescope. We took B- and R-band images of a $25'$ diameter around the group with the Wide Field Reimaging CCD Camera (WFCCD). The data were obtained on 2007 July 07 as part of an imaging campaign that covers all 12 HCGs in the J07 sample. The B and R filter exposure times were 300 s and 600 s, respectively.

These images allow for the detection of low surface brightness features, such as the signatures of past interactions, over a large area. We present this analysis in Figure 4, where we stacked the B and R images and applied a Gaussian smoothing filter to the result. This image shows only features and R-band contours that register at least 3σ above the background. We find two faint features, a 'bridge' that appears to connect galaxies A and B and an arc extending from B toward a compact structure to its north-west (we will later refer to this as the 'B-I arc'). There is another compact, extended source in the space between galaxies C and D.

The original purpose of the LCO observing program was to prepare a sample of dwarf galaxy candidates for spectroscopic follow-up. Though our redshift survey has yet to cover HCG 59, it is covered by the Sloan Digital Sky Survey (SDSS; York et al. 2000): a spectroscopic search sweeping a radius of 30 arcminutes around the nominal center of the group (the geometric center of the region enveloping the four known members) yields seven spectra with redshifts in the range 0.01–0.02: galaxies C and D and five compact galaxies. We therefore consider the membership of SDSS galaxies J114817.89+124333.1 and J114813.50+123919.2, which are covered by our wide-field imaging and J114930.72+124037.5, J114940.11+122338.6 and J114912.21+123753.8 which lie at projected distances greater than 13 arcminutes from the group center. The first of these galaxies is also present in the *HST* imaging, but lies partly in the ACS chip gap. In Section 4.1 we attempt to determine whether these are HCG 59 members through a phase-space analysis.

The Hickson (1982) naming convention assigns letters in order of brightness. Since our imaging does not cover all five dwarf candidates, we used the SDSS r-band photometry to consistently classify the galaxies as HCG 59 F through J. We have omitted the letter E, as it was assigned in the original catalog to a background galaxy. We attempted to measure stellar masses for these galaxies using 2MASS K-band images (Skrutskie et al. 2006), however, they are below the detection limit of that survey. Table 3 summarizes all of the information presented in this section: measured and SDSS photometry, radial velocities, galaxy morphologies and projected distances from the group barycenter. The latter two properties will be discussed in Section 4.1

2.6. *Spitzer* observations: infrared spectral energy distributions

The optical imaging was complemented by *Spitzer* imaging in the mid-infrared (IRAC 3.6–8 μm and MIPS 24 μm observations) presented in J07 and shown in Figure 5. In addition to the Rayleigh-Jeans tail of stellar photospheric emission, the IRAC bands probe the presence of hot dust and polycyclic aromatic hydrocarbons (PAHs), while the 24 μm observations trace cooler thermal dust emission. The dust and PAH emission are both stimulated by star formation activity. The harder spectra of active galactic nuclei typically destroy PAH molecules while heating dust to hotter temperatures than found in galaxies with star formation alone. At low AGN luminosities, the IR SEDs are often ambiguous (particularly in the presence of star formation; e.g., Gallagher et al. 2008).

The *Spitzer* images were combined with JHK_S observations from 2MASS (Skrutskie et al. 2006) to plot the IR spectral energy distribution (SED) of each galaxy (following J07), presented in the frequency-space plot of Figure 6. We have used the Silva et al. (1998) templates for galaxies of various morphological types. These map the SED of different galaxies as the sum of starlight and gas and dust emission from star formation and interstellar cirrus. We calculate the spectral index of the SED within the IRAC bands through a simple power-law fit. This was defined by Gallagher et al.
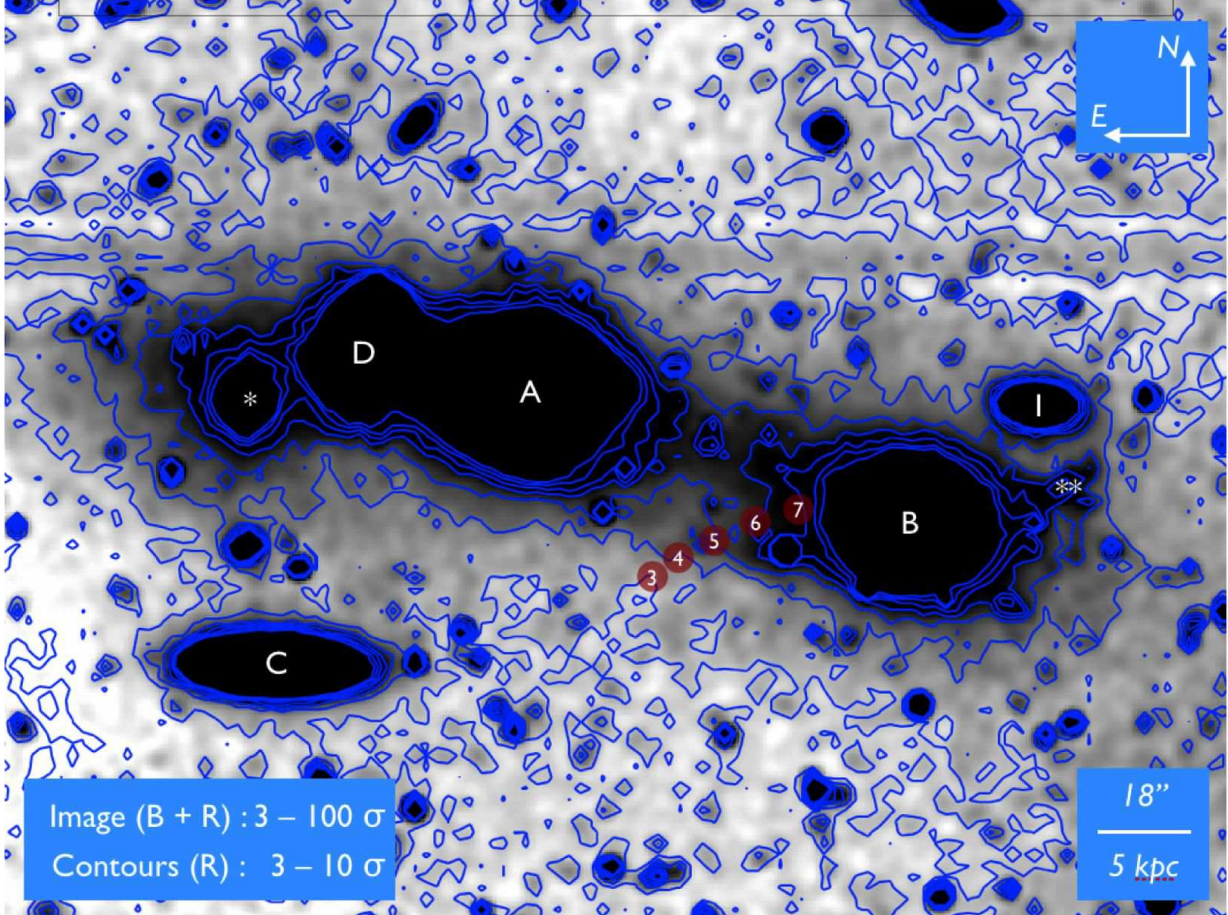
10

Fig. 4.— Co-added, smoothed, background-suppressed $B + R$ image of HCG 59 from the LCO duPont telescope. The image is aligned to the world coordinate system. The contours mark R-band fluxes between 3 and $10\,\sigma$ above the background (as marked by the circled numbers), while the smoothed $B + R$ flux shows material brighter than $3\,\sigma$ above the background level. The asterisk label denotes the foreground star to the east of galaxy D, while the double asterisk marks the H II regions west of B. The horizontal banding north of the main group is an artifact in the R-band image. We detect a streak of material apparently connecting galaxies A and B in our field of view. We argue in Section 4.3 that this is a *bona-fide* tidal bridge, although its low surface brightness prohibits an in-depth photometric study. A faint arc of light to the west of galaxy B – containing the H II regions mentioned above (see § 3.1) – appears to connect it with the dwarf galaxy I. We discuss the importance of these features in Section 4.3.

Table 3: Dwarf galaxies in HCG 59

ID	SDSS ID	(Plate, MJD, Fiber)	Morphology	r^a	$A_r{}^b$ (mag)	$M_r{}^c$	$v_R{}^b$ ($\mathrm{km\,s^{-1}}$)	d_{GC} (kpc)
F	J114930.72+124037.5	(1609, 53142, 464)	Sd	15.83	0.09	−18.15	3984	290
G	J114940.11+122338.6	(1609, 53142, 465)	dIr	17.34	0.08	−16.63	3195	471
H	J114912.21+123753.8	(1608, 53138, 625)	dIr	17.39	0.08	−16.58	4011	225
I	J114817.89+124333.1	(1608, 53138, 586)	dIm	17.43	0.10	−16.56	4038	32
J	J114813.50+123919.2	(1608, 53138, 593)	dE	17.69	0.10	−16.30	3942	83

[a]SDSS model r magnitudes. These values have not been corrected for Galactic extinction.

[b]Galactic extinction and recession velocities are from SDSS DR7.

[c]Absolute r magnitudes assuming a distance modulus of 33.89 and correcting for Galactic extinction.
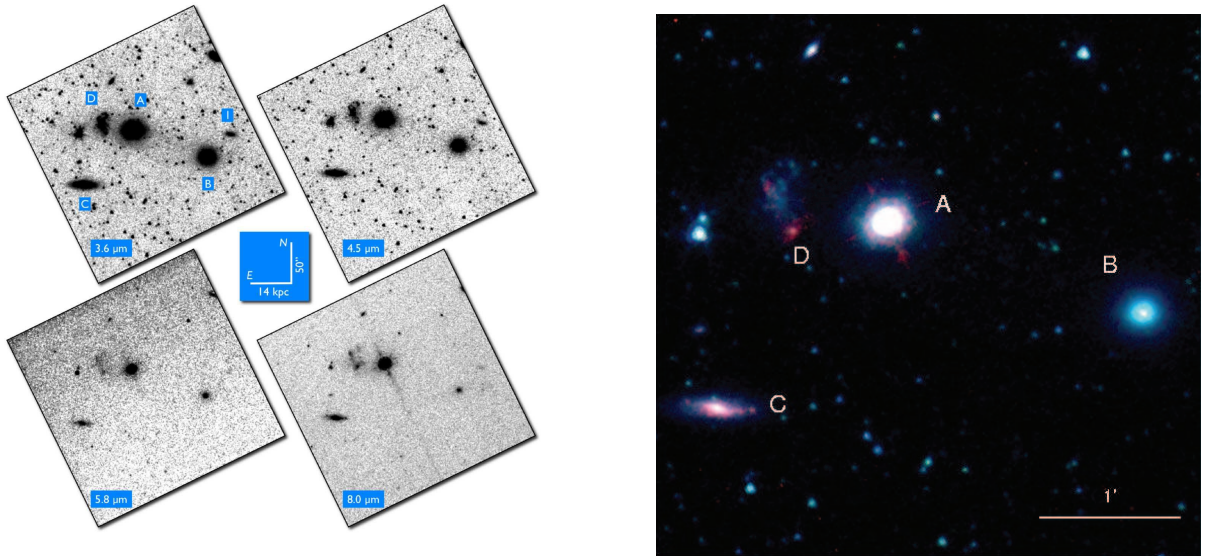

Fig. 5.— *Spitzer* 3.6–8 μm images of HCG 59. We present these individually to contrast the features evident in different bands and in a combined image to view the entire mid-IR picture. Galaxy A is extremely bright in the hot dust/PAH-dominated 5.8 and 8 μm bands. Galaxy B is faint in those bands, owing to little emission from heated dust. C is consistently bright in the four bands, given its ongoing star formation. D appears clumpy at long wavelengths, indicating patchy dust, heated by forming stars. In the 3.5 and 4.6μm images, we also see faint, diffuse emission in the region between A and B, which we study in Sections 2.5 and 4.3.

(2008) as α_{IRAC}, and it serves as a measure of star formation activity. In logarithmic frequency units, the flux difference from 8 to 4.5 μm leads to a positive gradient in quiescent environments, while star formation registers as a negative slope. For HCGs, the steepness of the slope is sensitive to the specific star formation rate (Tzanavaris et al. 2010).

In brief, the SEDs of galaxies B and C follow their morphological types of E/S0 and Sc, while the irregular nature of D does not allow for a template to be assigned (we use Sc in Figure 6). Galaxy A, nominally an Sa, shows strong excess light at wavelengths associated with PAH and/or hot dust emission ($\lambda \geq 5.8~\mu$m). If the flux in this region is associated with star formation, an Sc template would be more appropriate. This is, however, inconsistent with the optical morphology of A. Furthermore, the shape of this emission is also consistent with the AGN dust bump (e.g., Elvis et al. 1994; Gallagher et al. 2008), so in Section 4.5 we will examine the nuclear activity of this galaxy.

The SED-fitting process could not be carried out for the new dwarf galaxies catalogued in Section 2.5 due to the limited spatial coverage of the *Spitzer* imaging and the faintness of the dwarfs (they were not detected in 2MASS). As of July 2011, the Wide-field Infrared Survey Explorer (WISE) photometric catalogue did not cover HCG 59.

2.7. The high energy picture: *Chandra*-ACIS observations

The dataset is completed by *Chandra*-ACIS data in the 0.5–8.0 keV range. Results reported here are drawn from the work by Tzanavaris et al. (2011 in prep.). HCG 59 was observed by *Chandra* between 2008-04-12 and 2008-04-13 at the aim point of the back-illuminated S3 CCD of ACIS in very faint mode with an exposure time of 39 ks (observation ID 9406, sequence number 800743, PI S. Gallagher). The data were processed using standard *Chandra* X-ray Center aspect solution and grade filtering, from which the level 2 events file was produced. Figure 7 shows an adaptively smoothed 3-band X-ray image, with optical (I_{814}) contours overplotted for comparison.

`Wavdetect`, the `CIAO 4.1.2`[3] wavelet detection

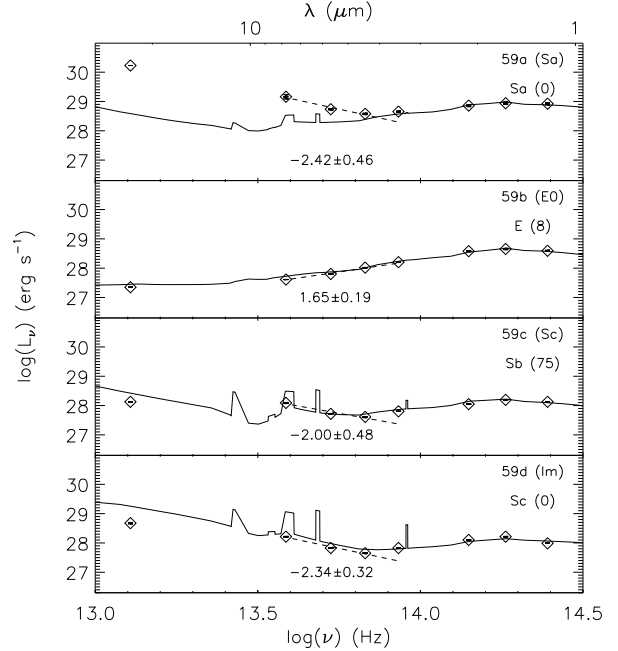[3] http://cxc.harvard.edu/ciao

Fig. 6.— Near-to-mid IR SEDs for the primary HCG 59 members. The photometric data, shown as diamonds, are drawn from 2MASS (JHK_s) and *Spitzer* MIPS/IRAC 3.5–24 μm (from J07). We annotate each panel with the morphological type from the literature (top row), as well as the type chosen to most accurately represent the data (bottom row). The bracketed number quotes the age in Gyr of the template for the elliptical, or the inclination in degrees of the spirals. We also cite the value of the α_{IRAC} diagnostic (Gallagher et al. 2008), which is fit on the wavelength range indicated by the dashed line. The solid curves represent GRASIL templates (Silva et al. 1998) appropriate for the morphological type of each galaxy (see text). Galaxies B and C are well represented by their nominal templates, while A and D deviate: in the case of galaxy D this is due to its irregular nature, while we consider the nuclear activity of A to be the source of the excess mid-IR emission (see Section 4.5 for details).
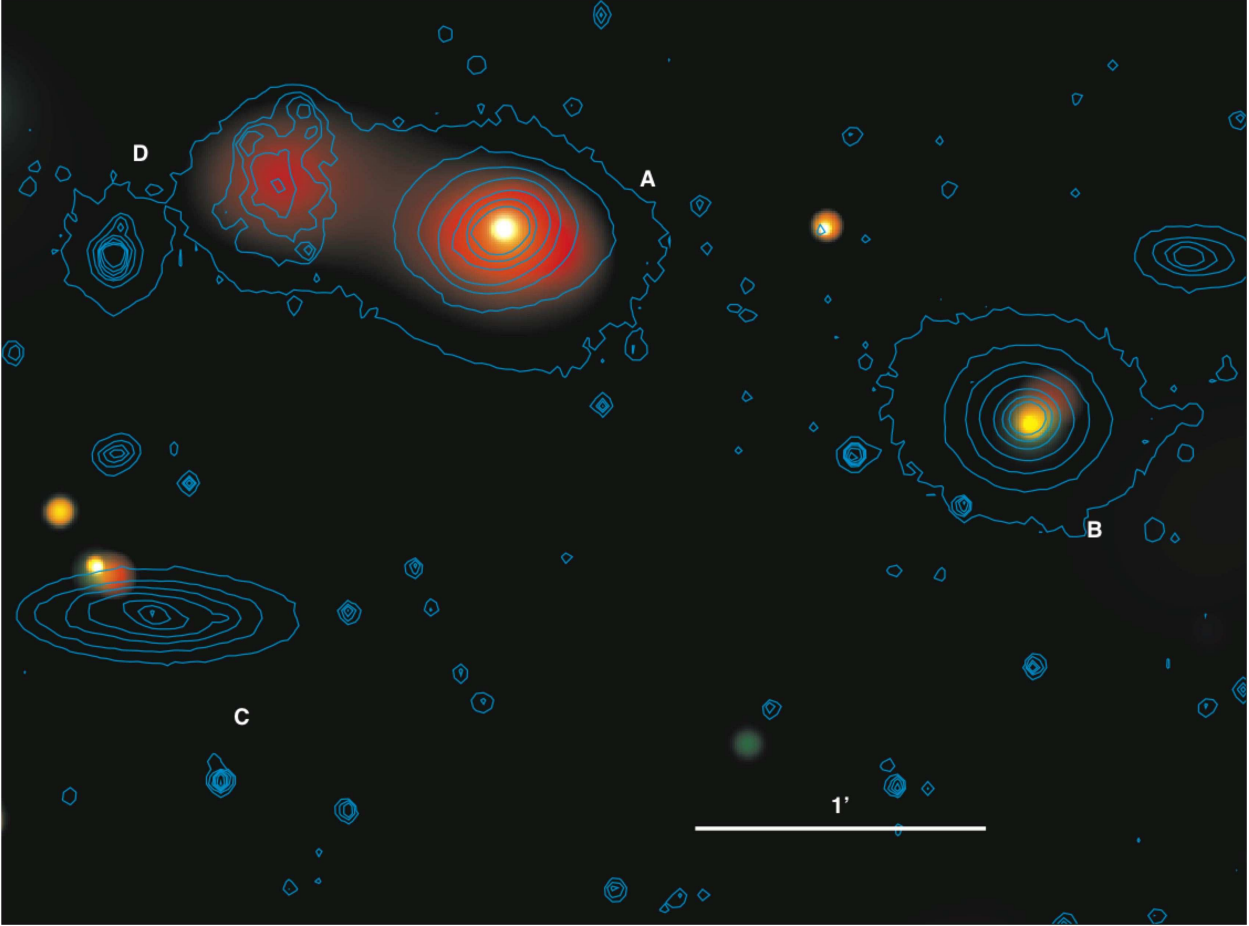
13

Fig. 7.— Adaptively smoothed three-band X-ray image of HCG 59, with overplotted I_{814}-band contours. Red, green and blue colors represent soft $(0.5 - 2$ keV), medium $(1 - 4$ keV) and hard $(2$–8 keV) X-ray emission. Galaxy C (Sc) has no detectable X-ray emission above the background level (the source at the limit of its optical isophotes is a likely background galaxy), while D (Im) shows some soft diffuse emission. The point source detected in the nuclear region of galaxy A (Sa) is detected in the full band with $L_{X(0.5-8.0)} = 1.1 \times 10^{40}$ erg s^{-1}. This is surrounded by diffuse emission. We resolve two point sources in the central region of Galaxy B (E/S0) with $L_{X(0.5-8.0)} = (1.4, 1.7) \times 10^{39}$ erg s^{-1}. Section 4.5 and Figure 17 provide details. No diffuse emission is detected from the intra-group medium.

14

tool (Freeman et al. 2002) was used in the soft (0.5–2.0 keV), hard (2.0–8.0 keV) and full (0.5–8.0 keV) bands to detect candidate point sources. The 1024×1024 S3 chip field was searched with `wavdetect` at the 10^{-5} false-probability threshold. Wavelet scales used were 1, 1.414, 2, 2.828, 4, 5.657 and 8.0 pixels. Source lists produced by `wavdetect` for each band were matched against each other by means of custom-made scripts (K. D. Kuntz, priv. comm.) to calculate a unique position for each candidate point source, taking into account the varying size of the *Chandra* PSF across the S3 CCD.

Point source photometry was carried out for the objects in the source list using `ACIS Extract`[4] (Broos et al. 2010) which takes into account the varying *Chandra* PSF accross the CCD. Poisson $\pm 1\,\sigma$ errors on net counts were calculated by means of the approximations of Gehrels (1986). Sources with measured net counts smaller than the $2\,\sigma$ error were flagged as non-detections. Note that this method produces very similar results to choosing a binomial probability threshold of 0.004 in `ACIS Extract` (Xue et al. 2011).

As sources have too few counts for reliable spectral fitting, we apply the method of Gallagher et al. (2005) to obtain a rough estimate of the spectral shape by using hardness ratios, defined as HR $\equiv (H - S)/(H + S)$, where H and S represent the counts in the hard and soft bands, respectively. Briefly, we use the X-ray spectral modeling tool `XSPEC` (Arnaud 1996), version 12.5.0, to simulate the instrumental response and transform observed HR values into an effective power law index Γ (where $f_X \propto E^{-\Gamma}$ photons cm^{-2} s^{-1} keV^{-1}), and also obtain associated X-ray fluxes and luminosities. This modeling includes neutral absorption from the Galactic $N_{\rm H}$ of 2.6×10^{20} cm^{-2} (Kalberla et al. 2005).

We estimate flux limits of $f_X \gtrsim 2.7 \times 10^{-16}$ erg cm^{-2} s^{-1} (0.5 - 2.0 keV) and $f_X \gtrsim 1.6 \times 10^{-15}$ erg cm^{-2} s^{-1} (2.0 - 8.0 keV), corresponding to luminosity limits of $L_X = 1.3 \times 10^{38}$ erg s^{-1} (0.5 - 2.0 keV) and $L_X = 7.7 \times 10^{38}$ erg s^{-1} (2.0 - 8.0 keV). Assuming these limits, we use the $\log N - \log S$ relation of Cappelluti et al. (2007) to estimate the number of background sources we would expect to detect in the HCG 59 field over

the 1.96×10^{-2} square degree area of the S3 chip. This number is ~ 25 and ~ 20 in the soft and hard bands, respectively, with a $\sim 20\%$ uncertainty. In the much smaller area (3.66×10^{-4} square degrees) covered by our galaxies, we expect < 1 background source in each band.

We detect a total of 40 sources in the soft band and 33 sources in the hard band over the ACIS S3 field. We thus expect about 15 soft and 13 hard sources to be point sources associated with HCG 59. We find that 9 soft and 3 hard sources are located inside the boundaries of the MIR-based HCG 59 galaxy regions of J07. We note that 11 sources that have only hard-band emission are located far from the HCG 59 galaxies and are thus likely background AGN.

In the central regions of two group galaxies, there are three notable X-ray point sources detected with high significance. As these point sources are all with $5'$ of the *Chandra* optical axis, the X-ray positions are the ACIS Extract "mean positions of events within the extraction regions"[5] with intrinsic positional uncertainties of a few tenths of an arcsecond. There is some additional uncertainty from matching the absolute reference frames of *Chandra* and *HST*, but this is expected to be small as both are consistent with 2MASS at the $\sim 0.1''$ level.

The first source, in galaxy A, has a full-band luminosity of $L_{X(0.5-8.0)} = 1.1 \times 10^{40}$ erg s^{-1} and an estimated $\Gamma = 1.3 \pm 0.3$. The X-ray position of this source is $0.7''$ from our quoted optical position (Table 1). This isolated point source in the nuclear region of galaxy A has a luminosity that is consistent with known low-luminosity AGN (e.g., Ho et al. 2001) and significantly higher than individual, luminous X-ray binaries. The two point sources found in the central region of galaxy B have X-ray positions $0.2''$ and $1.3''$ from the *HST* i-band galaxy centroid position (Table 1). Unfortunately, these sources have fewer than 10 counts in each band, precluding even a rough Γ estimate. Their full-band luminosities are $L_{X(0.5-8.0)} = (1.7, 1.4) \times 10^{39}$ erg s^{-1}, respectively.

The *Chandra* images are also sensitive to diffuse emission from MK degree gas. As can be seen in our adaptively smoothed image, some soft, diffuse

---

[4]http://www.astro.psu.edu/xray/docs/TARA/AE.html

[5]See Section 5.3 of the ACIS Extract User Manual – http://www2.astro.psu.edu/xray/docs/TARA/ae_users_guide.html

emission is detected in galaxy D (Im), likely associated with star formation, as well as in galaxy A. In both cases, the diffuse emission covers an area several times the size of the *Chandra* PSF at that location. We obtain an upper limit on the IGM surface brightness as follows. We calculate the count rate in a source-free region between group galaxies, and estimate the corresponding flux for $kT = 0.5$ keV thermal emission using PIMMS.[6] We thus estimate the IGM surface brightness to be $\lesssim 7.3 \times 10^{-17}$ erg cm^{-2} s^{-1} arcsec^{-2}. Finally, we note that dwarf galaxy I is not coincident with any detected X-ray sources; none of the other new dwarf members of HCG 59 are within the *Chandra* field of view.

We will discuss the implications of these observations further in Section 4.

3. The young and old star cluster populations: star formation over a Hubble time

3.1. Young star clusters and the past $\sim$ Gyr of star formation

The population of star clusters is representative of star formation as a whole in any system (e. g. Bressert et al. 2010). They are formed *en masse* after large events (e.g., Trancho et al. 2007; Konstantopoulos et al. 2008, 2009; Konstantopoulos 2009; Bastian et al. 2009) and at a slower pace at all times when a galaxy is forming stars (Lada & Lada 2003). The extreme brightness of young clusters makes them detectable to large distances and therefore a reliable tracer of the star formation history of their host galaxy over a Gyr or so. Beyond that point in time they are referred to as intermediate age clusters and eventually globular clusters. As a whole, the cluster population of a galaxy can reveal its star-forming history over a Hubble time.

In this section, we analyze the cluster populations of the four main galaxies in HCG 59 using the *HST* PSF photometry described in Section 2.2. We use color-color (CC) and color-magnitude (CMD) diagrams to roughly age-date the clusters by comparing them to evolutionary tracks. The *BVI* filter combination of our *HST* images lacks coverage below $\sim$ 4000 Å, which is

crucial to breaking the age-reddening degeneracy (owing to the inclusion of the Balmer jump and near-UV continuum). However, it is still possible to infer the passing of intense bursts of star formation via the clumping of data-points along the evolutionary track, and unreddened young clusters are clearly evident.

Figures 8 through 11 show the high-confidence sample (*i. e.* clusters with $M_V < -9$ mag; see Section 2.2) as solid dots, while the extended sample is marked with open triangles. The solid and dashed red lines (running top to bottom) show Marigo et al. (2008) evolutionary tracks for simple stellar populations (SSP) of $\frac{1}{5}$ Z$_\odot$ and Z$_\odot$. This is slightly different from our previous work, where we used Bruzual & Charlot (2003) models. We made this change because the Marigo et al. (2008) models seem to provide a good fit to both young clusters and globulars, unlike other model suites which focus on one part of the cluster population. The green lines that run more or less horizontally show Starburst99 (SB99; Leitherer et al. 1999) tracks of the same metallicities. These also include nebular emission, which we expect to often be present during the first $\sim$ 10 Myr of evolution. At this state the cluster is still surrounded by residual gas from the time of its formation ionized by UV photons. This short-lived phase ends when the first stars evolve and explode in supernovae that expel the gas. Clusters with colors redder than 0.8 in both axes are most likely GCs, although they might be highly reddened young clusters.

When contrasting the extended and high-confidence samples, the former appears to spread more in color-space. This reflects a mass effect intrinsic to star clusters, rather than indicating contamination. Two recent studies, Silva-Villa & Larsen (2011) and Popescu & Hanson (2010), independently reached the conclusion that lower mass (fainter) clusters, $M \lesssim 10^4$ M$_\odot$, often exhibit deviations from the theoretical model tracks. In this mass regime, the underlying stellar initial mass functions (IMF) are under-sampled and stochastic effects dominate the overall light. Given that the IMF is populated randomly, it is physically equivalent to creating either one high mass star, or $\sim$ 100 low mass stars (given the IMF slope). In contrast, a high-mass cluster will populate the IMF fully. Consequently, a population of high-mass clusters will have smaller intrinsic pho-

---

tometric dispersion. A cluster with lower mass will run out of material before the IMF becomes fully sampled, thus leading to the presence of gaps and spikes. Because of this effect, the presence of a high mass star in a low mass cluster will make the cluster appear to have a larger photometrically derived mass than one with only lower mass stars.

We now treat the population of each galaxy individually. In the following paragraphs, all star and globular cluster candidates discussed are taken from the high-confidence sample. The distinctions of young, intermediate, and globular are inferred from the locations of candidates along evolutionary tracks within the B_{435}–V_{606} vs. V_{606}–I_{814} color-color space.

Galaxy A (Sa) hosts a very small detectable population of five GCCs and two intermediate-age cluster candidates. The CMD shows them all to be consistent with having high masses, with $\log(M/\mathrm{M_\odot}) > 5$. The lack of young clusters, combined with the high masses of the ones detected, indicates that galaxy A has stopped forming stars at a high rate. Because the mass-to-light ratio of a stellar population increases with age (*i. e.*, the older a cluster becomes, the higher its mass must be for detection), young clusters should dominate the cluster population when the SFR is high. The non-detection of *any* young clusters is further evidence that the UV+IR emission is dominated by AGN continuum, and the inferred SFR of 5 $\mathrm{M_\odot}$ yr^{-1} is severely overestimated.

Galaxy B (E/S0) hosts mostly red clusters; the GCCs vastly outnumber young cluster candidates in this system. In fact, the four SCCs in the high-confidence sample do not strictly belong to galaxy B, but are found in the IGM: two nebular sources are located in a clump to the west of the galaxy, which we are treating as part of a stream that connects this galaxy to the dwarf HCG 59I in our field of view. We will return to these H II regions in Section 4.3. The two non-nebular SCCs are distinct clusters in dwarf galaxy I. This means that the presence of patchy dust (as seen in the *HST* images of 59B) by itself is not indicative of star formation at a high enough level to produce massive clusters, consistent with its SFR of 0.02 $\mathrm{M_\odot}$ yr^{-1}.

Galaxy C (Sc) shows a continuous star formation history, evident in the smooth distribution of

datapoints along the evolutionary track. The presence of nebular sources indicates some current star formation, while the low masses ($\approx 10^4$ $\mathrm{M_\odot}$) derived throughout the sample imply an overall low level of star formation over time. This is in accord with the low value of 0.16 $\mathrm{M_\odot}$ yr^{-1} for the SFR of the galaxy. There is no pronounced GC population.

Galaxy D (Im) is an unusually large irregular galaxy. It shows a continuous star formation history through to the present. The CMD shows a handful of SCCs with $\log(M/\mathrm{M_\odot}) \gtrsim 5$. At 0.48 $\mathrm{M_\odot}$ yr^-1, this galaxy has the largest SFR of those with young clusters. There is no old component in the cluster distribution, no evident halo of GCCs, again possibly due to the low mass of the system which implies a small globular cluster system. Furthermore, the extended sample does not reveal a tight, correlated color distribution characteristic of GCs. The youngest clusters lie at a typical color-space distance of ~ 0.3 mag away from the nebular model track along the reddening vector, indicating the presence of dusty star-forming regions.

3.2. Star cluster complexes

One step above star clusters in the star formation hierarchy is cluster complexes, large agglomerates of young stars, arranged in a fractal distribution that follows the collapse of the progenitor gas. These structures can be used to understand the global star formation activity in a galaxy. They are found to be more compact at higher redshifts than in the local universe (with two to five times higher mass surface density, as found by Elmegreen et al. 2009), although in one local interacting compact group, HCG 31, we find complexes to be similar to those at intermediate redshifts (Gallagher et al. 2010). We argue in this series of papers that compact groups might process gas more efficiently when interacting than most other environments apart from the infall regions of galaxy clusters (Walker et al. 2010). HCG 31 fits well in that context.

Star-forming complexes are extended amorphous regions, with dust scattered across their surfaces. Their boundaries were identified by eye and measured by contours down to a limiting surface brightness about 10σ above the background. We single out 30 star-forming complexes in this
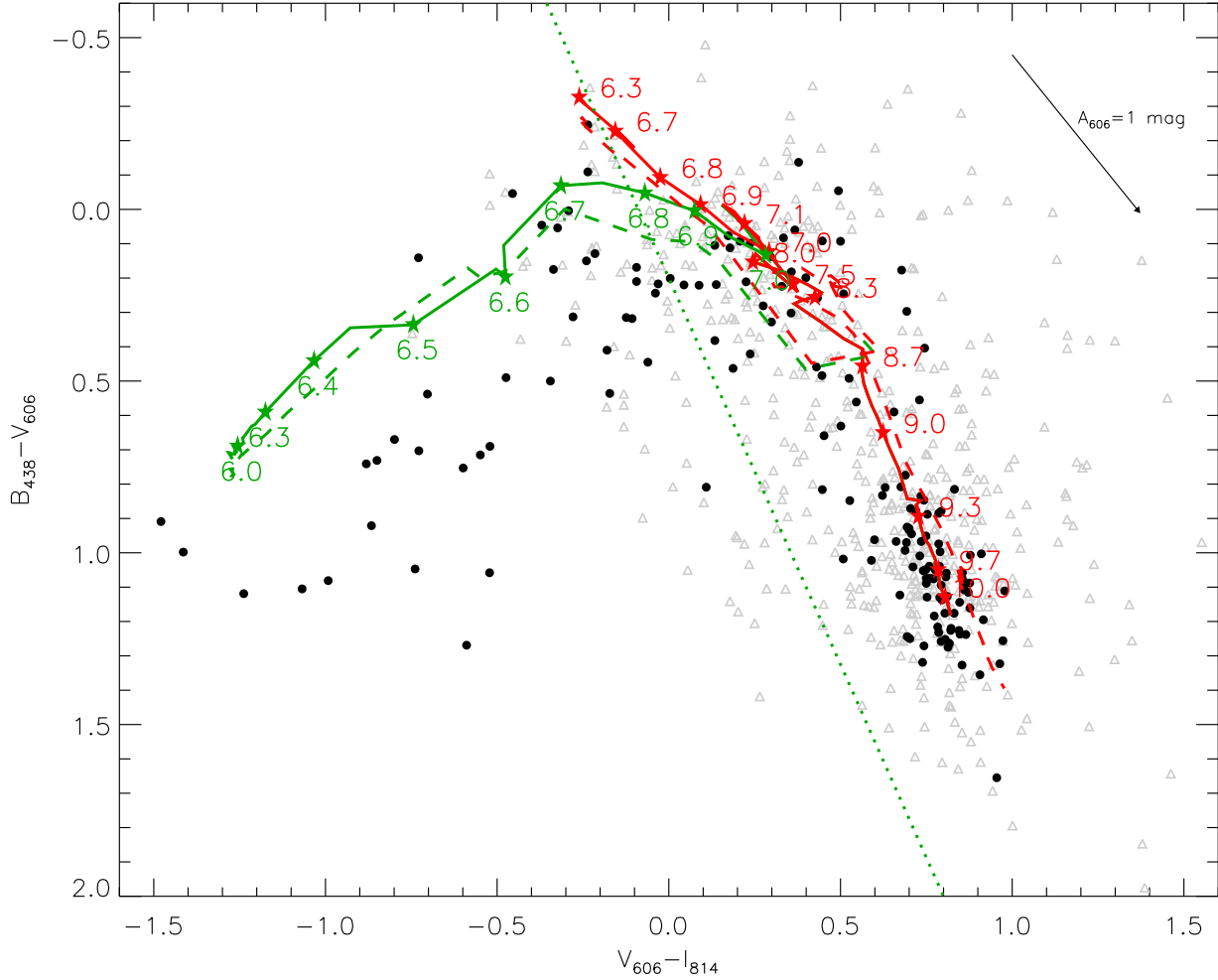
Fig. 8.— $B_{435}-V_{606}$ *vs.* $V_{606}-I_{814}$ colors of all SCCs in HCG 59, plotted along with $\frac{1}{5}$ $Z_\odot$ (solid red line, bottom) and $Z_\odot$ (dashed red) model tracks by Marigo et al. (2008), spanning an age range of 6 Myr to 13 Gyr (indicated by filled stars). The green lines (solid and dashed for $\frac{1}{5}$ $Z_\odot$ and $Z_\odot$) show a Starburst99 track that accounts for nebular emission, as suited to the very youngest clusters that have not yet expelled their natal gas. Data-points that lie to the left of the dotted green line are considered 'nebular', *i. e.* younger than ~ 10 Myr. The high-confidence sample of SCCs (those with $M_V < -9$) is denoted by solid dots, while open triangles show fainter candidates comprising the extended sample (all cluster candidates to the detection limit). Much of the spread in the extended sample colors is due to stochasticity in populating the stellar initial mass function within clusters, as discussed in the text. We also indicate an extinction vector of length $A_{606} = 1$ mag. We will present the distribution of each galaxy separately in the next figure.
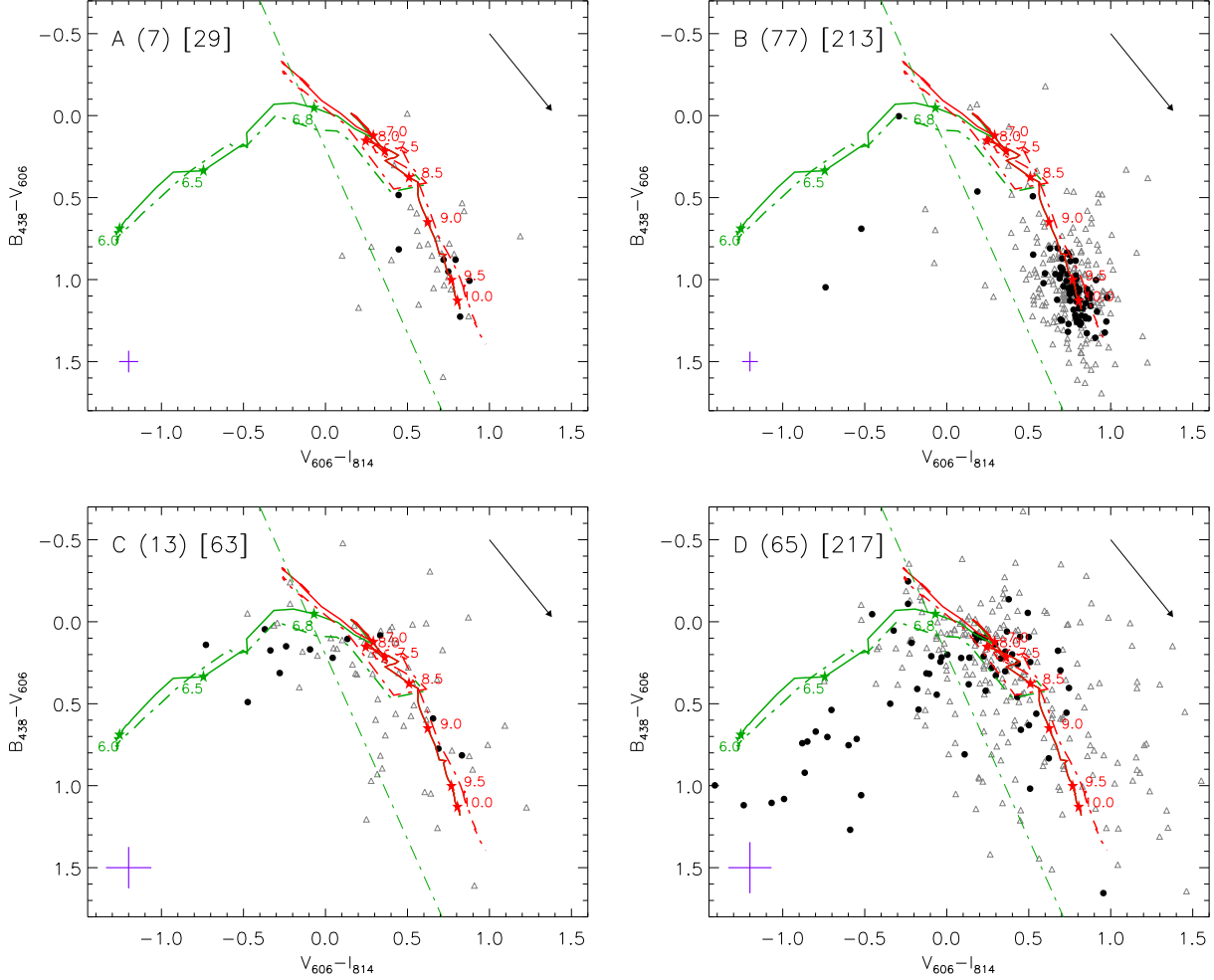
Fig. 9.— $B_{435}-V_{606}$ *vs.* $V_{606}-I_{814}$ colors of SCCs, divided by galaxy, following Figure 8. Typical error bars are indicated as crosses in the lower left part of each plot. The irregular galaxy D is the only one that displays pronounced current star formation activity, as deduced by the number of nebular sources – although more nebular sources could be hidden behind dust and gas in the highly inclined spiral galaxy C. Galaxies C and D are consistent with continuous star formation histories over the course of their histories. The absence of GCs in D might indicate the galaxy is young, although it could be due to the fading of its low-mass cluster population below our detection limit (which is a function of age). Galaxies A and B only appear to host globular clusters and a handful of intermediate-age and young clusters, indicating quiet star formation histories over the past Gyr or so.

19
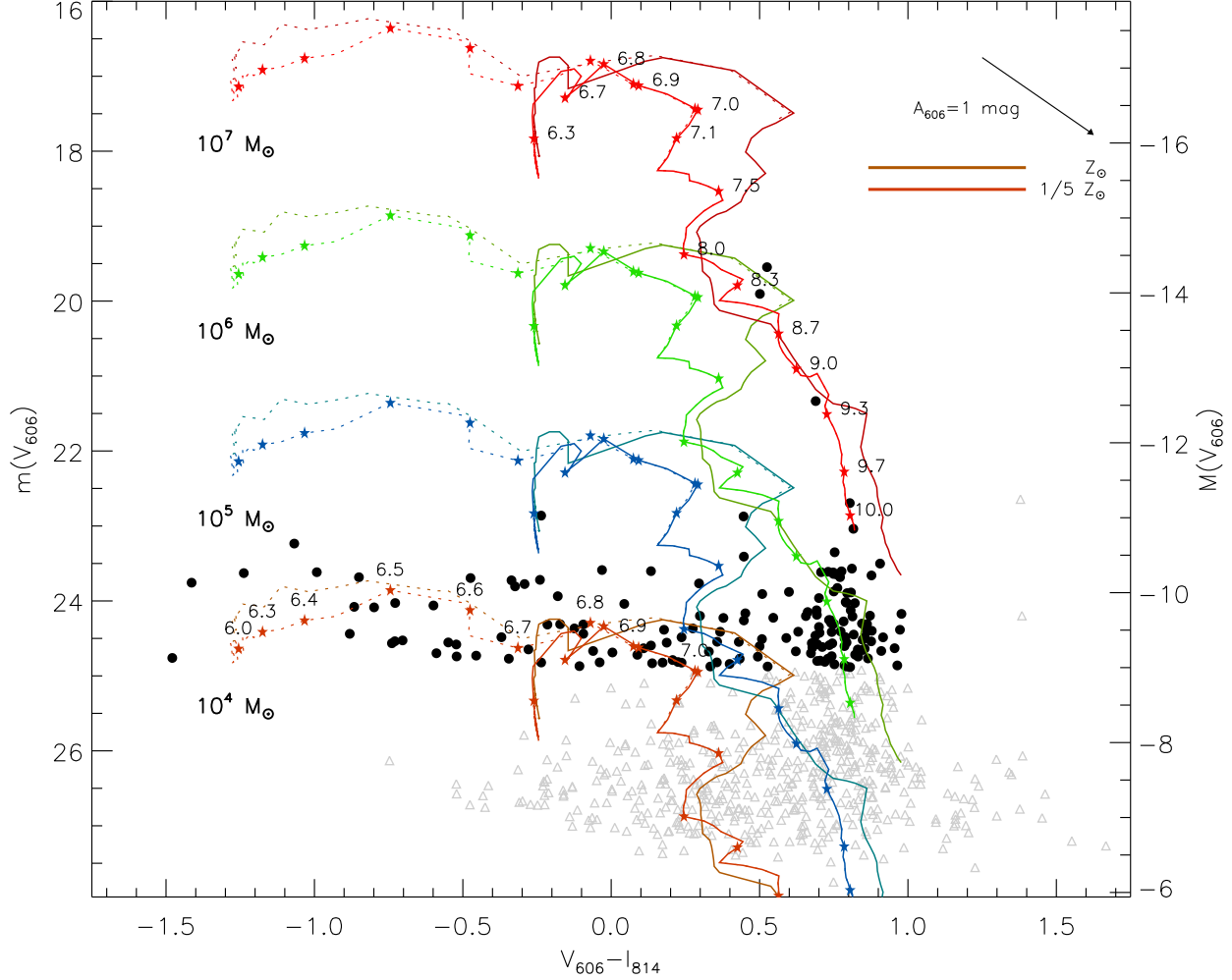
Fig. 10.— V_{606} *vs.* $V_{606}-I_{814}$ color-magnitude diagrams, following the datapoint plotting conventions of Figure 8. We have provided Marigo et al. (2008) model tracks for four different cluster masses, times two metallicities, $\frac{1}{5}$ $Z_{\odot}$ and $Z_{\odot}$ (top and bottom) (solid lines), with the 'nebular' tracks plotted as dotted lines. As in Figure 9, the age increases from top left to bottom right. In both samples, we tentatively deduce typical cluster masses – with the caveat that mass and extinction are degenerate – of $\lesssim 10^4$ $M_{\odot}$, with an additional locus of possible 10^6 $M_{\odot}$ clusters. This distribution is consistent with local cluster populations, given the imposed cut-off for the high-confidence sample at $M_V < -9$ (and therefore the lower limit of $\sim 10^4$ $M_{\odot}$).
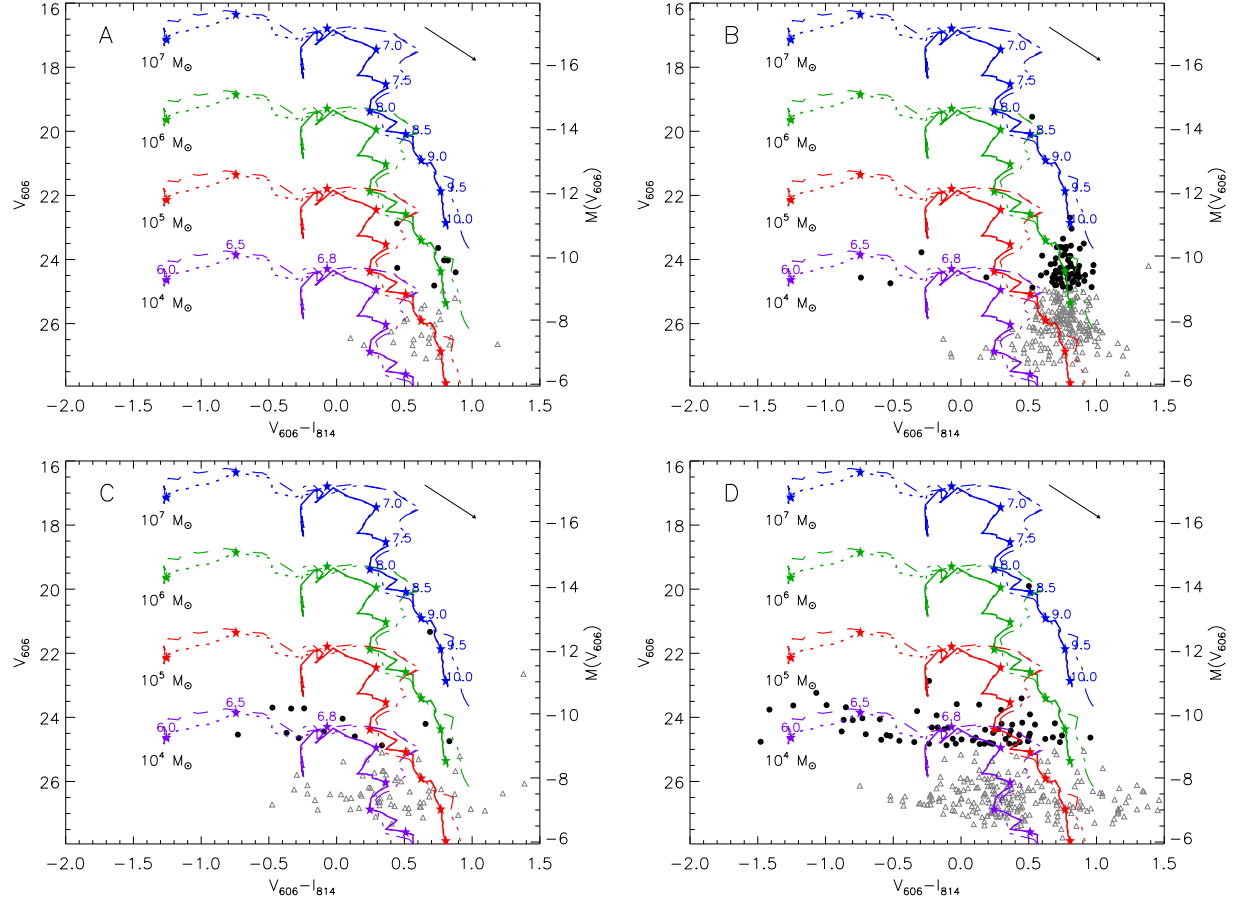
20

Fig. 11.— V_{606} *vs.* $V_{606}-I_{814}$ color-magnitude diagrams for each galaxy individually, following the plotting conventions of Figure 10. Galaxy B is notable for the large population of apparently old, massive ($\sim 10^6$ M$_\odot$) clusters, while galaxy D has shows a sizable population of 10^4 M$_\odot$ clusters consistent with a predominantly young and intermediate-aged system.

21

compact group, three in galaxy C, and 27 in D. We find no complexes in the E/S0 galaxy B or A, the evolved (Sa) spiral. The sizes of these complexes are comparable to those in local systems (Figure 12; *cf.* Elmegreen et al. 1994, 1996) and consistent with HCG 7, a relatively inactive compact group (Konstantopoulos et al. 2010). Their colors are indicative of star formation and nebular emission, as expected of star-forming regions (Figure 12, right). In all, the star-forming complexes in HCG 59 are comparable to their counterparts in local star-forming galaxies. They follow very closely a relation between brightness and size, much more so than we found in our previous study of HCG 7. We show this correlation in Figure 12 (right) where the line is a simple linear fit to the data. The linear fit implies a similar surface brightness for complexes across the group, unlike in HCG 7, where we found significantly more scatter.

3.3. The ancient globular cluster systems of HCG 59

Globular clusters represent the earliest eras of star formation in a given galaxy. Their color distributions carry the imprints of interactions and mergers and thus may probe the history of their hosts over a very long timescale.

In this section we provide a full analysis of the number and color distributions of the GC populations in HCG 59 and complement the star formation and interaction histories we began to explore in Section 3.1. This analysis is built around the plots of Figure 13. The top row has a color-color plot (left) and histogram of the $(B-I)_0$ distributions (right) in each galaxy. (The color-magnitude diagram is shown in the left panel Figure 3.) Owing to their projected proximity, the GC systems of galaxies A and D overlap, and so we cannot provide separate analyses. However, given the relative masses of the two galaxies and their evolutionary stages, it is safe to assume that the population is dominated by A.

We find a fairly large population of globular clusters across this compact group, the vast majority of which are found in and around B. Recall that given the fading of clusters with age, GCs need extremely high masses, $M \gtrsim 10^5$ M$_\odot$, to be detected to such large distances. We also find some clusters at large radial distances from the center of

this galaxy, including some found along the stellar stream that appears to connect galaxies A and B (see Section 4.3) and its projection on the far side of galaxy B. Galaxies A and C host small populations. To quantify these populations, we derive the specific frequency, S_N, a measurement of the number of clusters per unit galaxy luminosity, for each galaxy. First, we correct the observed number of GC candidates by the background correction noted above, and then calculate the total number of GCs expected around each galaxy by first adopting a photometric completeness fraction of $f = 0.9 \pm 0.1$ for objects with $V_{606} < 26$, and correcting for the expected fraction of GCs that lie below this magnitude limit. The S_N values are 0.3, 7.7 and 0.1 for galaxies A, B and C respectively, assuming that all bright GCCs consistent with the halo of A are actually bound to A. The measured and derived numbers are collected in Table 4.

The size of the population in galaxy C is consistent with its Sc morphological type, while B has a tremendously rich system, about twice the number of GCCs expected. Conversely, the GC population of galaxy A is much poorer than expected, compared to the values of $S_N \sim 1$ typically seen in Sa spirals (Chandar et al. 2004). Many of the detected GCCs appear to lie in a ring just outside of the bulge of the galaxy. Comparing to other GC populations in HCGs, our specific frequency for HCG 59B of $S_N = 7.7 \pm 3.0$ is larger than (yet still consistent within the uncertainties) those observed so far in other large elliptical galaxies in HCGs: global values of $S_N = 3.6 \pm 1.8$ for HCG 22A from Da Rocha et al. (2002),[7] and $S_N = 4.4 \pm 1.3$ for HCG 90C from Barkhouse et al. (2001).

Inspection of the region marked 'outer B' in Figure 3 shows a possible excess of GC candidates over the background level described above in Section 2.4, perhaps tracing an intra-group stellar population. This is not unusual, as compact groups by their very nature are likely to promote interactions. (White et al. 2003) detected diffuse intragroup emission in HCG 90 accounting for up to half the light of the group. Two further studies, Da Rocha & Mendes de Oliveira (2005) and Da Rocha et al. (2008), found intra-group light in

---

[7]The lower $S_N \sim 1.7 \pm 1.0$ from Barkhouse et al. (2001) for HGC 22 A is due to their larger M_V for the galaxy – both studies find a very similar total number of globular clusters.
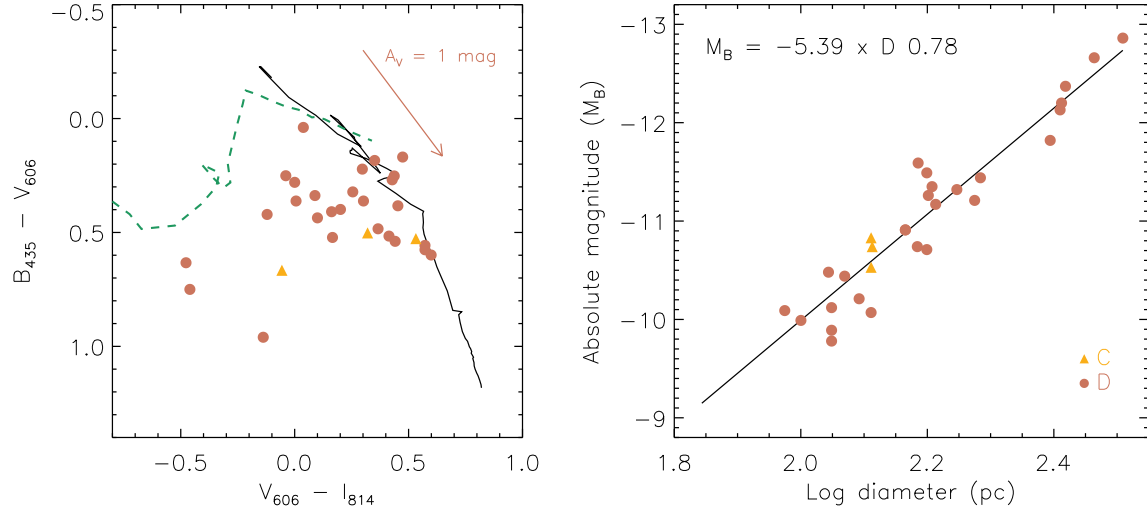
Fig. 12.— Color-color and size-luminosity $(D - M_B)$ diagrams for star cluster complexes in HCG 59. The plotting of the evolutionary tracks follows the conventions of Figure 8. Complex symbols are coded to indicate where they are found: galaxy C (filled, yellow triangles) or D (filled, orange circles) The colors of the complexes are indicative of star formation, as expected. We find the complexes to follow a linear luminosity-size relation (see the upper left corner of the right-hand panel) very well. This implies a similar surface brightness for complexes across the group, unlike in HCG 7, where this relation is not obeyed.
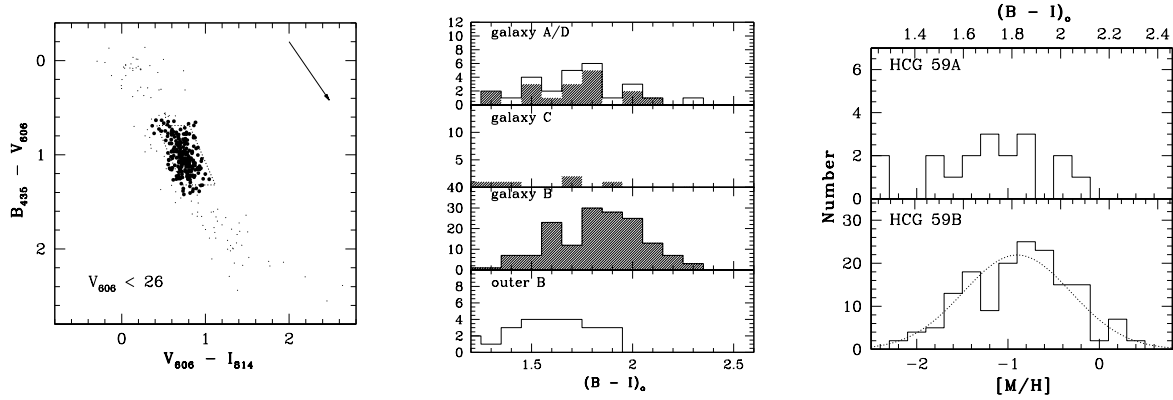
Fig. 13.— **Left:** Color-color diagram of all detected GCCs. The dotted parallelogram on the left shows the selection box, based on the colors of GCs in the Milky Way (Harris 1996). **Center:** $(B - I)_0$ distribution for all detected GCCs. The shaded area in the plot of the A/D distribution omits GCCs superposed over the body of D. The 'outer B' distribution covers all GCCs in pointing 2 that are at least 15 kpc from the centre of galaxy B. This region might suffer from some contamination, although it is consistent with observed distributions of GCs, which show a tendency for red clusters to be at large galactocentric distance as would be expected for a halo population. On the **right**, we relate the color distribution to that of metallicity and compare galaxies A and B directly. The dotted line in the GC metallicity distribution of galaxy B shows a best fit Gaussian, which we plot since a more complex distribution is not statistically justified.

another six groups: HCGs 15, 35, 51, 79, 88, and 95. In HCG 59, a total of $N = 15 \pm 4$ GCCs lie within the 2.7 arcmin^2 region, where we expect a background contribution of 6 ± 2 objects. Assuming only Poisson noise, this suggests a $\sim 2\sigma$ excess of objects in this part of HCG 59. This possible excess could be due to variations in the stellar density in the Galactic halo or the Sgr Stream. However, the luminosity function of this small number of sources in the 'outer B' region (shown as the solid line in the right panel of Fig. 3) is weighted towards the faint end, suggesting that at least some of these objects are indeed true GCCs located far ($\sim 25 - 50$ kpc) from galaxy B. The unusually large population of GCCs associated with B, the anomalously small population in A, and the possible population of GCs in the IGM (presumably stripped from a member galaxy), all indicate that this compact group environment may have redistributed GCs between member galaxies and/or to the IGM.

In particular, possible interactions in the recent history of galaxy B might have redistributed its GC system. With this in mind, we compare the azimuthally averaged radial profile of the spatial distribution of the GC system with the surface brightness profile of the galaxy, as derived through GALFIT (Peng et al. 2010b). The galaxy is best fit by a single-component Sérsic profile of shape $n = 3.1$. Interestingly, we find the Sérsic profile of the galaxy to provide a better description of the GC system than the best fitting power-law profile of index -1.3. This is contrary to the finding of power-law GC system distributions around loose group member NGC 6868 and HCG 22 A. If that is to be considered the norm for compact groups, then perhaps the recent interaction activity about galaxy B has changed the shape of its GC halo.

The bottom panel of Figure 13 shows the $(B - I)_0$ color distribution (converted to the Johnson photometric system for direct comparison to Galactic globulars) of the clusters in each galaxy. The shaded area in the plot of A/D shows clusters that are clearly part of A, i. e. omits the ones that are projected upon the body of D. This does not alter the distribution, strengthening our assumption of a small population in D. Galaxy C also hosts a very small population, as expected due to its low mass.

The color distribution can act as a proxy of

metallicity for GCs and we take advantage of that to compare the two populous distributions of galaxies A and B. The color distribution of galaxy A seems fairly flat and the low numbers do not allow for a statistical treatment. Galaxy B, however, provides a large enough population to perform a test for bimodality, using the KMM algorithm of Ashman et al. (1994). This returns no evidence for a composite distribution in the metallicity distribution.

4. Discussion

4.1. Extending the membership of HCG 59

In Section 2.5 we introduced a search for dwarf galaxies in HCG 59, which we continue here. Since all objects we are considering here are covered by SDSS, we will not provide images and spectra here. More information can be obtained from the SDSS database using the plate IDs, Modified Julian Dates (MJDs), and fiber IDs given in Table 3.

Regarding the morphologies of the new members, I, the candidate covered by our *HST* imaging, seems irregular, with a peaked light profile. This agrees with its spectrum, which shows clear emission lines and a continuum shape typical of a spiral. We classify it as dIm. The rest of the galaxies are not covered with high-resolution imaging, so we are more conservative in classifying them. F shows quite clear spiral structure in the SDSS images, and is therefore given an Sd type. We note that its star formation seems to be declining, given that Hα is the only detectable emission line. G and H appear quite irregular and elongated, with spectra exhibiting blended emission and absorption. We assign them dIr types. Finally, J shows a morphology closer to spherical and weak emission lines (although the S/N does not allow for a confident determination); we assign it a dE type.

Regarding their roles as group members, four of the five galaxies do not appear to be interacting with any other members, as might be expected from their locations far from the group core (Figure 14, left). It is only I that shows some evidence of an interaction with galaxy B, in the form of the 'B-I arc' described in the Section 2.5. This stellar stream includes the large star-forming region we find to the west of galaxy B, which is part of the

Table 4: Observed and derived properties of the globular cluster systems in HCG 59

Galaxy	N_{GCC}[a]	N_{back}[b]	$N_{V<26}$[c]	N_{total}[d]	S_N [e]
A	18±4	6±1.0	13±6	33±21	0.3±0.2
B	162±13	6±1.0	180±34	462±182	7.7±3.0
C	7±3	6±1.0	1±3	3±8	0.1±0.3
D	11±3	1±0.2	11±5	28±18	1.6±1.0

[a]Number of detected GCCs

[b]Background correction

[c]Number of clusters brighter than $V = 26$ mag

[d]Estimated total GC population

[e]Specific frequency

analysis of Section 3.1.

In order to assess whether these galaxies belong to the group, we perform a phase-space analysis, following the statistical studies of Mulchaey & Zabludoff (1998) and Zabludoff & Mulchaey (2000). This is shown in Figure 14, right panel, where each datapoint represents a dwarf galaxy. The x-axis measures the distance of a galaxy from the group centroid, calculated as the mass-weighted average position of the four main members (A through D). The y-axis shows the offset of a galaxy's radial velocity from the group mean, normalized to the core group (A through D) velocity dispersion of 314 km s^{-1}.

We find all galaxies to satisfy our membership constraints. Four of five spectroscopically detected galaxies lie within the boundary set by the four main members; galaxy G, which has the largest offsets in physical and velocity space, is moving with a radial velocity offset less than three times the group dispersion. We therefore consider all five galaxies under consideration here to be members of HCG 59, based on a strict 3σ-clip, as demonstrated in Figure 14. The inclusion of new members updates the velocity dispersion of the group to 335 km s^{-1}. Based on this value, we derive a dynamical mass for HCG 59 of $M_{dyn} = 2.8 \times 10^{13} \text{ M}_\odot$, a $\sim$ 10-fold increase with respect to the main members alone. This in fact changes the J07 evolutionary stage of the group from Type II (intermediate) to Type III (gas-poor), as it yields a ratio of H I-to-dynamical mass of 0.71, with the caveat that the measured H I mass is likely underestimated because the dwarfs at large group radii are not included.

It is interesting to find dwarf galaxies at large distances from the center of the group. This lack of barycentric clustering is also observed in the Local Group, where it is seen as a morphology-density relation: dwarf irregulars (dIr) are found at larger distances from the group center (Grebel 1999) than the quiescent dwarf spheroidals (dSph) and dwarf ellipticals (dE). This may indicate that some dIrs are galaxies experiencing their first infalls to the group center. Such a situation could explain the relatively large velocity offset and the star-forming nature of galaxy G.

The membership of galaxy G seems the most uncertain of the five galaxies discussed above, given the marginal agreement with the 3σ velocity cut, and the large projected barycentric distance. This is important, as its inclusion does affect the updated dynamical properties, due to the large change in group radius. We quantify this in Table 5, where we summarize the dynamical properties of HCG 59. Those numbers show a change of mass by a factor of ~ 4 or ~ 10 with and without galaxy G, while the J07 type changes from II to III regardless of the inclusion of G. The velocity dispersion is most affected: including G increases the value to 336 km s^{-1} from the original 314 km s^{-1}, while excluding G significantly reduces the dispersion to 208 km s^{-1}, which is more consistent with the evolved state suggested by our analysis.

4.2. The current state of star formation

We have presented several diagnostics of star formation activity across HCG 59. The Tzanavaris et al. (2010) SFRs of galaxies A through D are $\simeq$ $[4.99, 0.02, 0.16, 0.48] \text{ M}_\odot \text{ yr}^{-1}$. These are de-
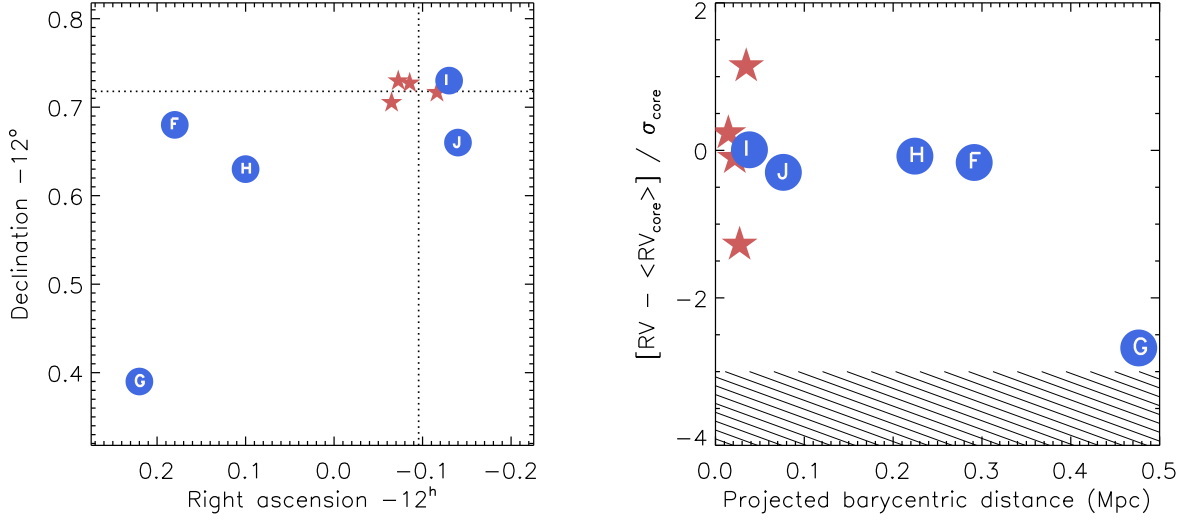
Fig. 14.— Diagnostic diagrams of dwarf galaxy membership. The **left** panel shows the positions of the dwarfs and giant galaxies as blue dots and red stars respectively. We have labelled the dots with the appropriate lettering for HCG members. On the **right** we present a phase-space diagram that plots the offset of a galaxy's radial velocity from the established group mean (σ_{core}, the line of sight velocity dispersion of the giant galaxies) against its distance from the group barycenter (mass-weighted centroid). Four of five spectroscopically detected dwarfs lie within the boundaries set by the main galaxies and as such are confirmed as members. The fifth is moving at a relative radial velocity less than three times the group's velocity dispersion and is therefore also included as a member. The lower boundary of this $3\,\sigma$-clipping criterion is shown on the plot as the shaded area.

Table 5: Updated dynamical properties of HCG 59

Reference	$\bar{v}$	σ_v	M_{dyn}	J07 type
	($\mathrm{km\,s^{-1}}$)		($\mathrm{M_\odot}$)	
Hickson (1982)	4036	314	2.9×10^{12}	II
This work	3924	336	2.8×10^{13}	III
This work, excluding G	4015	208	1.1×10^{13}	III

termined from the combination of UV and IR light assuming that all of the light emanates from star-forming regions. The presence of young star clusters in galaxies C and D shows that stars are forming at a fair pace, in accord with the star formation rates quoted in Table 1. Overall, the SFRs are consistent with the infrared SEDs of these galaxies with the notable exception of A which is almost certainly strongly contaminated by AGN emission and shows no evidence of ongoing star formation from the other evidence on hand. There are several soft X-ray point sources throughout the group, which are likely to probe compact stellar remnants local to HCG 59 galaxies. There is also soft, diffuse X-ray emission confined to the galaxies, which probes $\sim 10^6$ K gas heated by star formation (stellar winds and SNe). The IR images do not show much that is surprising: emission along the spiral arms of C and in the star-forming clumps embedded in D. Four of the five dwarf galaxies show star formation activity, J being the exception. They are found to be star-forming based on either their bright emission lines or blue continua. Galaxies A and B, on the other hand, exhibit quiescent or even extinguished star formation. In the case of A, this is inferred by the absence of young star clusters.

In all, the group does not appear to be undergoing a burst or any other event notable in terms of current star formation. With the exception of the two most massive galaxies, the group is forming stars at a regular pace. This is also exemplified by the behavior of star cluster complexes across the group, which follow very closely after a brightness-radius relationship consistent with typical nearby galaxies, and in contrast to HCGs 7 and 31 (Konstantopoulos et al. 2010; Gallagher et al. 2010).

4.3. Signatures of interactions in the intra-group medium

Major interaction or merger events are very often accompanied by bursts of star and cluster formation. The examination of star clusters in HCG 59 presented in Section 3.1 did not show any evidence of such events in the last few Gyr. Given the high mass-detection limit for star clusters at this distance, they cannot be used to trace minor dynamical events. We therefore search for such evidence in the lowest surface brightness features

detectable in our LCO images. In Section 2.5, we reported the detection of a low surface brightness stream of material in the projected area between galaxies A and B. This is visible at low surface brightness in our *HST* imaging and quite pronounced in the wide-field images from Las Campanas, at the $> 3\,\sigma$ level. We also detected an arc of luminous material to the west of galaxy B, perhaps connecting it to compact galaxy I, which we discuss in Section 4.1.

The low surface brightness and limited extent of the 'B-I arc' preclude precision photometry. We can therefore only pursue an in-depth analysis of the bridge between A and B. In order to derive the photometric properties of this feature, we first drew a color-map to look for an evident $B - R$ gradient. Unfortunately, the stream is not bright enough to clearly dominate the image background. We thus conducted photometry of the area and the outskirts of the two galaxy that bracket it. We used large apertures of radius 75 pc (8 px) to reduce the background noise. The results are plotted in Figure 15; on the left panel we compare the measured photometry with the evolution of the $B - R$ color, according to the Marigo et al. (2008) model tracks of three metallicities. We find an intermediate value between the colors of the outskirts of the two galaxies that define this region (plotted as yellow dashed lines), cautioning that the emission in this region might be affected by the two galaxy light-envelopes to some extent.

The origin of the bridge is not clear and its faintness makes it difficult to ascertain the dominant source of emission. It could consist either of stripped stars, or stars that formed *in situ* from stripped gas. If this is mixed stellar material from the two galaxies, we cannot study it in any more detail. We can, however, develop the *in situ* formation scenario further, by treating the bridge as a simple stellar population. In this case, the color-magnitude diagram of Figure 15 (right), provides an age estimate of about 1 Gyr, depending on metallicity. In addition, the CMD plotted in this figure provides an estimate of the stellar mass contained: with 10^7 M$_\odot$ of ~ 1 Gyr old stars in each aperture, we extrapolate a mass in the order of $\sim 10^8$ M$_\odot$, *i.e.* a density of ~ 100 M$_\odot$ pc^2. If the stars here are stripped from a galaxy, the overall mass will be higher, as the M/L of simple stellar populations increases with time.
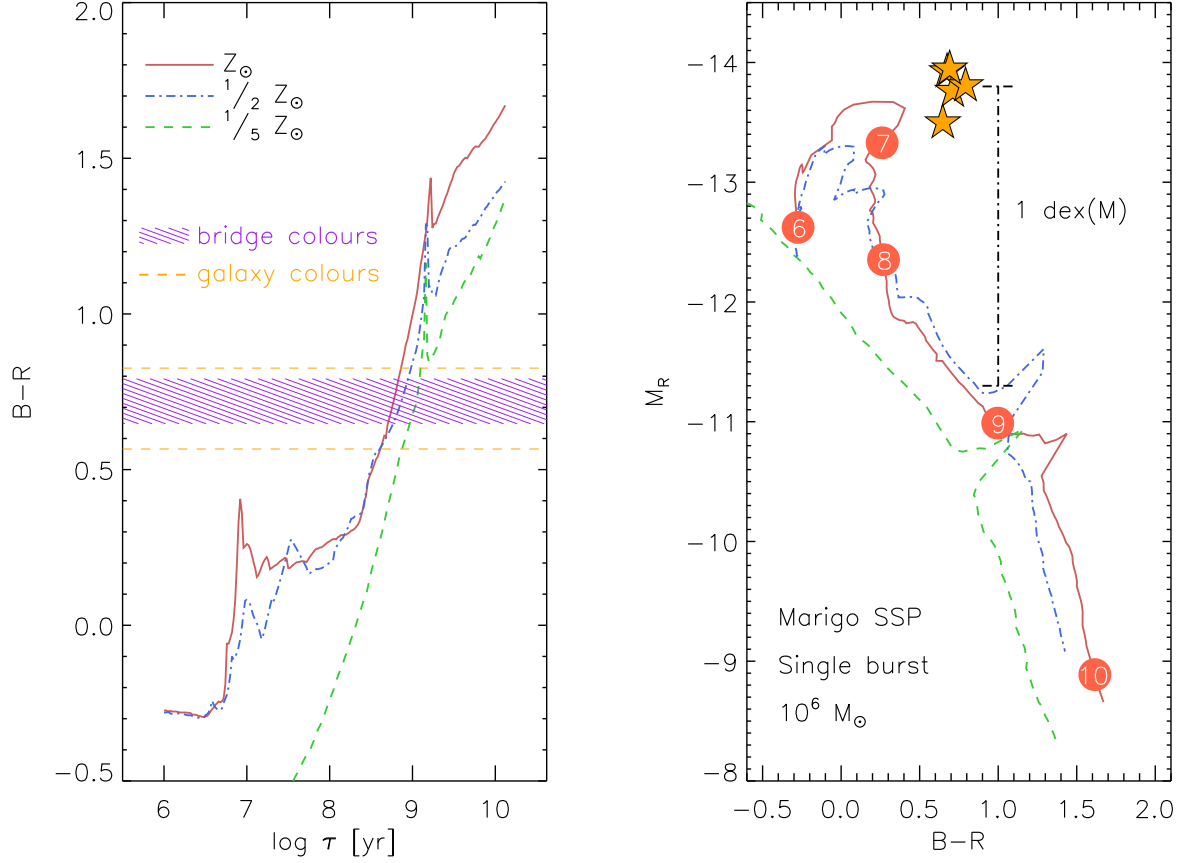
Fig. 15.— Diagnostic plots of the tidal bridge between galaxies A and B. The age-color plot on the **left** shows the evolution of the $B - R$ index over time ($\log \tau$), for Marigo et al. (2008) models of three different metallicities: $\frac{1}{5}$, $\frac{1}{2}$ and solar, shown as dashed green, dashed-dotted blue and solid red lines respectively. The range of colors in the bridge, as measured in five successive apertures and shown as a shaded region, lines up with the tracks at ages around 1 Gyr (depending on metallicity). The photometry of this faint feature might be affected by diffuse light from the galaxies, which brackets that of the bridge (denoted by dashed yellow lines, galaxy A is the bottom line). A secondary diagnostic is presented on the **right**, in the form of a color-magnitude diagram. The numbered dots denote log age in years, while the stars show the color and magnitude of each bridge aperture. If this is a simple stellar population (see text), then we can extrapolate a mass of $\sim 10^8$ M$_\odot$ over the ~ 1 kpc^2 area of the bridge. This measurement can provide constraints for models of the evolution of tidally induced stellar structures.

28

4.4. HCG 59B as a merger remnant

HCG 59B, the E/S0 galaxy on the west side of the group, seems quite regular at first glance, however, a close inspection of the low-level light reveals some interesting features. While *ELLIPSE* fitting shows an overall smooth isophotal structure in B_{435} light, there is severe isophotal twisting in the central regions. This is spatially co-incident with several patches of extinction we detect in the *HST* images; they are most pronounced in B_{435}, observable in V_{606} and hardly detectable in I_{814}, implying a thin column of dust. In the *Spitzer* bands, the fits indicate very symmetric structure in the 3.6 and 4.5 μm bands, but the 5.8 and 8.0 μm fits show a faint cusp some ~ 7 px, or ~ 2.5 kpc from the $r^{-1/4}$ surface brightness profile peak.

The color-composite IRAC image (Figure 5) shows hints of structure in galaxy B; however, an evolved elliptical/lenticular with near-zero star formation should present a smooth isophotal profile in all bands. Nonetheless, its SED (Figure 6) shows a gradual decline, indicative of emission from stellar photospheres, rather than the heated dust associated with star formation.

To investigate these irregularities further, we take advantage of the high resolution of the *HST* images. We construct pixel-by-pixel color maps of B, with the aim of tracing the exact location of the extinction patches. If the underlying stellar population is evolved to the same stage (*i. e.* an evolved SSP), then extinction will be the only source of discrepancies in color. There are, in fact, three possible sources of color variations in this filter combination: (i) extinction across a similarly colored stellar population (mixed or coeval); (ii) spatially separated stellar populations of various ages and/or metallicities; or (iii) the presence of gas and star formation – *i. e.* H II region emission lines.

The maps, shown in Figure 16, cover the three possible filter combinations; for reference, the V_{606} image is also shown. The $B - I$ map is the one most sensitive to extinction. To quantify, the Cardelli et al. (1989) extinction law assigns almost twice the extinction in the B_{435} as it does to the I_{814}, $A_{435}/A_{814} = 1.85$ ($A_{435}/A_V = 1.13$, *cf.* $A_{814}/A_V = 0.61$). This is therefore the map we use to detect patches of low extinction, of order 0.3 mag, in three fingers extending approximately eastwards from the north-south line through the nucleus. This faint structure is seen in all three colormaps, but not in the V_{606} image. The *F606W* filter covers various emission lines, including Hα, [N II], [S II], Hβ, and [O III]. Interestingly, Martínez et al. (2010) found Hα, [NII] and [SII] emission in the spectrum of B, at relative intensities consistent with a composite H II region plus AGN emission. From the concentrated, blue core of the $V - I$ image, this line emission appears to be spatially coincident with the nucleus.

Circumstantial evidence for a close encounter in the recent history of galaxy B is provided by the uneven distribution of its GC system. GCs normally form spherical haloes, however, here we find GCs at large radii, many concentrated along the stellar stream that seemingly connects galaxies A and B, and its extension across the far side of galaxy B. Furthermore, the overabundance of GCs in galaxy B is matched by a severe dearth of clusters in A. Given the possibility that the two galaxies interacted ~ 1 Gyr ago, a scenario whereby GCs are transferred between the two systems is not out of the question. It is unclear from a dynamical perspective why in the process of an interaction the GCs would flow from A, the more massive entity, to B. In a simple thought experiment, we move as many clusters from B to A as are required to level the S_N of A to the nominal value for an Sa. This still leaves an excess of GCCs in B relative to normal. However, the factor-of-two uncertainties involved in the determination of S_N do not rule out this scenario of GC 'swapping'.

The X-ray map of this galaxy, as described in Section 2.7, reveals two distinct X-ray sources in the nuclear region. Unfortunately, with full-band luminosities of $L_X = (1.4, 1.7) \times 10^{39}$ erg s^{-1}, neither is sufficiently luminous be identified as an unambiguous AGN – a possibility that the optical spectroscopy of Martínez et al. has indicated. Given the lack of ongoing star formation in the region, the sources are unlikely to be high mass X-ray binaries, though luminous low mass X-ray binaries (associated with older stellar populations) or groups of them unresolved at the distance of HCG 59 are plausible. In addition, due to the uncertainty in matching X-ray sources to optical imaging, we cannot confidently derive a one-to-one correlation between the optical clumps and these
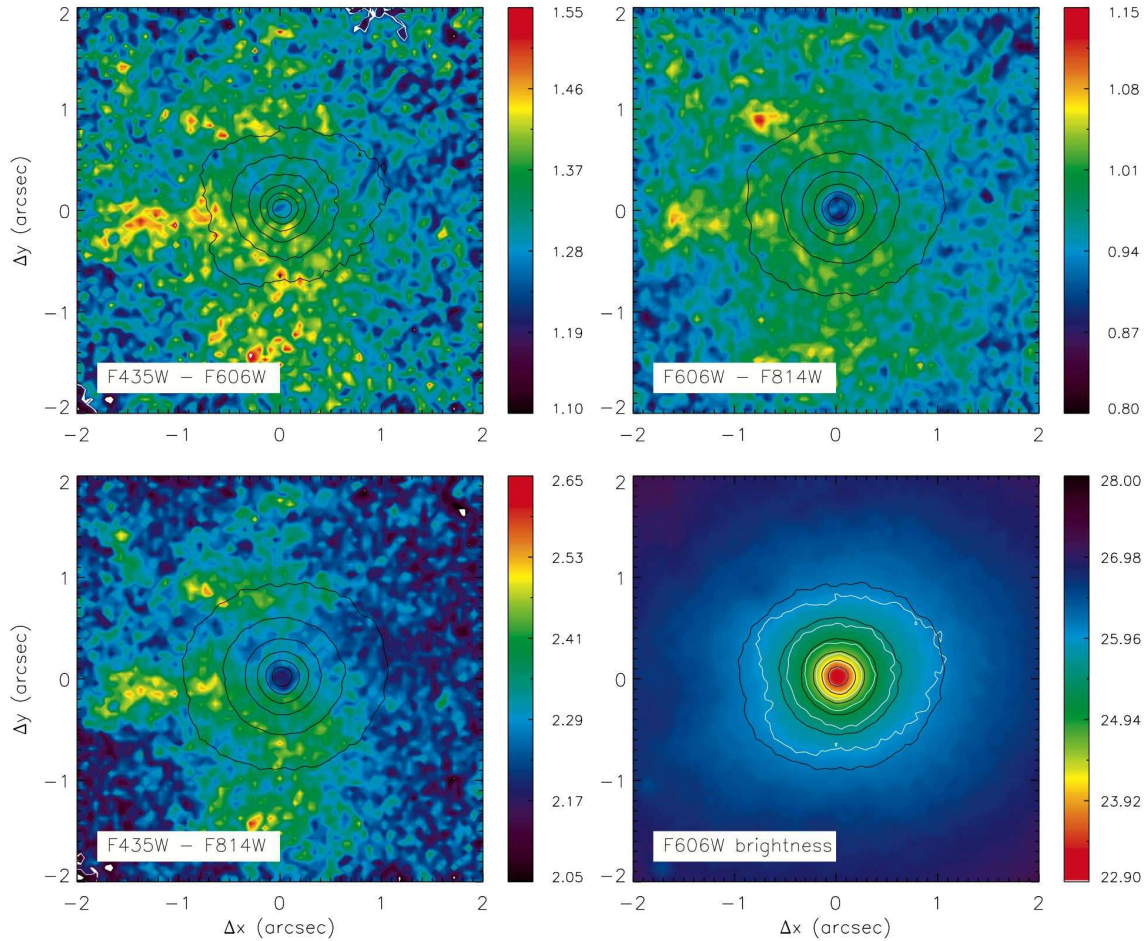
Fig. 16.— *HST* color maps of the central region of HCG 59B. The maps are centered on the nucleus, defined as the peak of the I_{814} surface brightness profile, and aligned to the world coordinate system, with north to the top and east to the left. The bottom right map shows the V_{606} brightness. Contours show B_{435}, V_{606}, I_{814}, and I_{814} flux in the four panels (upper left, upper right, lower left, lower right). Each successive contour maps a difference in brightness of 0.5 mag. The $B - I$ map on the bottom left is most sensitive to extinction and does indeed show patches of moderate reddening. The top row maps also show the extinction patches evident in the bottom row. In both the $V - I$ and $B - I$ color maps, the nucleus appears bluer than the surroundings; this is consistent with additional flux from line emission in the B_{435} (Hβ) and V_{606} (Hα) filters. The meaning of the observed colors is discussed in more detail in Section 4.4.

sources, although the correlation is confirmed to within the X-ray positional uncertainties. We note however that, as discussed in Section 2.7, the nuclear X-ray sources are spatially close to the optical center of the galaxy.

The excess of globular clusters and uneven dust distribution in the nuclear regions of B hint at some interaction in the more distant ($>$ Gyr) past, but the lack of additional evidence for structural disturbances limits our ability to infer more. We do detect a few young clusters in galaxy B and a non-zero (though low) SFR, and therefore some reservoir of cold gas is present. Accretion of a satellite galaxy is therefore a possibility. Furthermore, the unimodal GC color distribution does not favor a gas-rich, major merger in the past. This conclusion follows the paradigm of Muratov & Gnedin (2010), who attribute the known bimodality of GC colors to late-epoch mergers. It is also a reasonable assumption that the implied interaction did not feature a major merger with a gas-rich system, as that would have enhanced the young and intermediate-age cluster populations.

4.5. Nuclear activity in HCG 59A

In Section 2.6 we reported that the IR emission in galaxy A is consistent with being dominated by an AGN, rather than star formation. This is based on the disparity between the galaxy's morphological type of Sa and the high UV+IR SFR suggested by interpreting the emission as related to SF. Furthermore, the lack of young massive clusters is inconsistent with a SFR of 5 $M_\odot$ yr^{-1}.

This hypothesis is supported further by the finding of a hard X-ray source in the nuclear region of galaxy A, with $L_X = 1.1 \times 10^{40}$ erg s^{-1} as reported in Section 2.7. The spectroscopic AGN survey of HCGs (Martínez et al. 2010) places the galaxy at the interface of the H II and AGN zones in the 'BPT' diagram (Baldwin et al. 1981), based on optical emission-line ratios. The 2$''$-wide slit they used encompasses a wide region (effective aperture of 0.58 kpc), therefore the signal is most likely diluted by circumnuclear and disk light. Visual inspection of the central region reveals asymmetric structure, resembling a second nuclear source of comparable I_{814} luminosity to the nucleus. As in the previous section, we employ *HST* color maps to take advantage of the spatial reso-

lution of $\simeq 12$ pc per pixel.

The maps, shown in Figure 17, reveal a cone of blue light at $(x, y) \simeq (-0.1, 0.1)$, with colors of $B_{435} - V_{606} \simeq 0.9$, $V_{606} - I_{814} \simeq 0.6$, and $B_{435} - I_{814} \simeq 1.6$. The complexity of the central region inhibits easy interpretation, but one clue are the emission lines covered in the three bands. V_{606} covers Hβ, [O III], Hα and [N II], which can be associated with star formation and/or AGN activity. In this scenario, the blue cone could stand out as a result of geometry, perhaps being located in a break in the dust distribution. A simple explanation could relate this feature to an unreddened line of sight through the inner spiral structure of A. In that case, however, we would expect to see bright, young star clusters, as they are known to shine through thick columns of dust, let alone relatively dust-free regions (e. g. Region B in M82; Smith et al. 2007; Konstantopoulos et al. 2008).

A different interpretation can relate this structure to an AGN. The lack of symmetry could suggest a small narrow-line region, photoionized by the AGN continuum, with projection effects and obscuration hiding the cone on the far side. This would produce strong [O III] and [N II] emission, the presence of which was reported by Martínez et al. (2010). This geometry is consistent with the inclination of galaxy A of no more than 30° (assuming the AGN and galaxy share the same inclination angle).

Combining the pieces of evidence collected from the X-ray, optical and MIR emission, we propose that the nuclear emission in HCG 59A is dominated by a low-luminosity AGN with a photoionized narrow-line region. The onset of activity may be related to a possible encounter with galaxy B about 1 Gyr ago, as tentatively dated from the colors of the bridge connecting the two galaxies (Section 4.3).

5. Summary

We have presented an analysis of HCG 59, a compact group comprising four main galaxies and at least five newly discovered dwarfs at the $M_r < -15.0$ mag level. Our results are based on multi-wavelength observations and continue a series of papers that have followed two different approaches: on the one hand we have treated the overall properties of Hickson compact
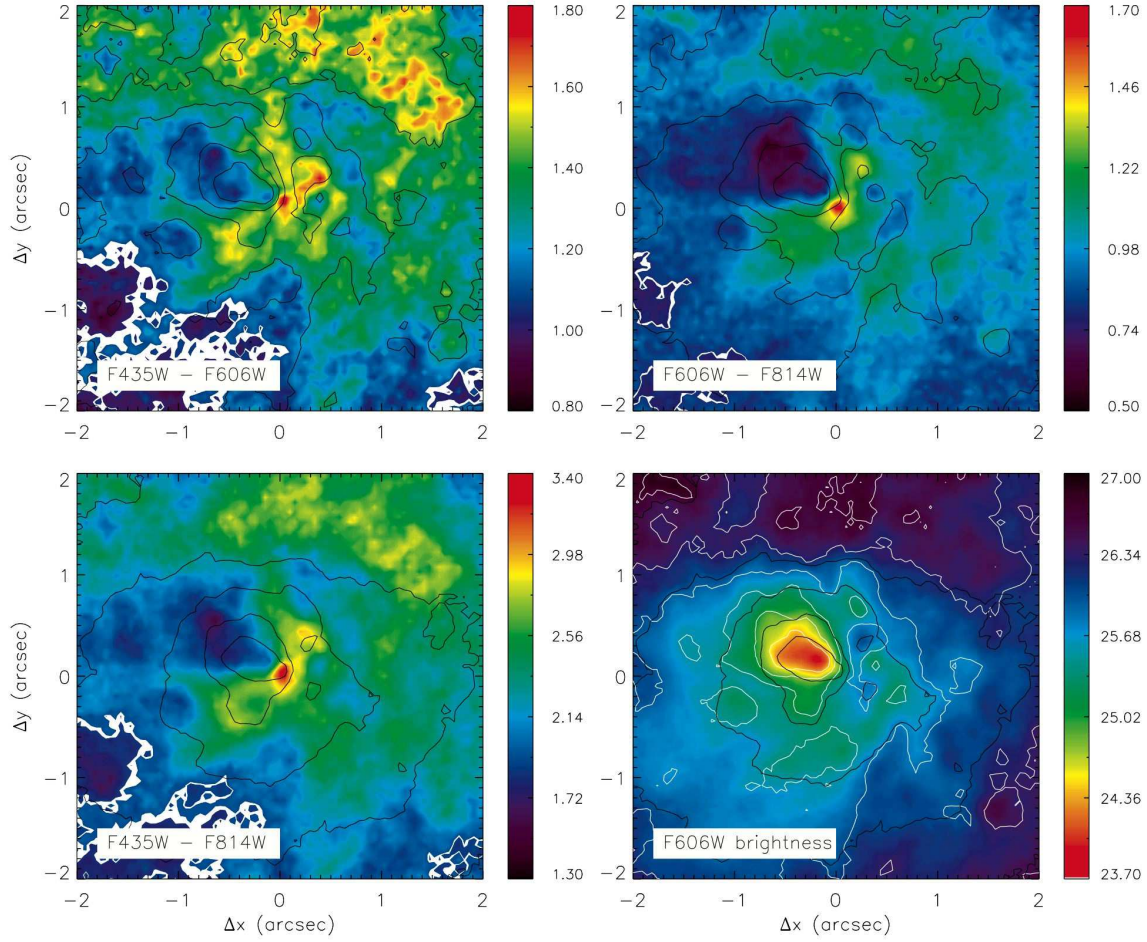
Fig. 17.— *HST* color maps of the nuclear region of HCG 59A, following the plotting technique presented in Figure 16. North is to the top and east is to the left. The central peak appears elongated in the V_{606} flux map (lower right) and shows a composite structure with two additional peaks nearby and a long tail. The tail could be an artifact introduced by the complex and heavy extinction in this region, perhaps caused by the inner spiral structure of HCG 59A. It could alternatively be associated with the nuclear activity we note in the X-ray image of this galaxy (Section 2.7), as well as the significant excess in 8 and 24 μm emission, discussed in Section 2.6. A blue cone-shaped structure is most evident in the V_{606}–I_{814} color map (top right). The nature of this blue cone is discussed in Section 4.5.

groups (Johnson et al. 2007; Gallagher et al. 2008; Tzanavaris et al. 2010; Walker et al. 2010); on the other hand, we have surrounded our *HST* observations with a multi-wavelength dataset to pursue in-depth investigations of individual CGs, one at a time (Palma et al. 2002; Gallagher et al. 2010; Konstantopoulos et al. 2010).

Compared to HCGs 7 and 31, two compact groups previously studied in this series, HCG 59 presents something of an intermediate step: where HCG 7 was found to be interacting solely in the dynamical sense (*i. e.* currently in the absence of direct hit encounters), HCG 59 shows evidence for stronger interactions in the recent past. There is evidence for star formation in the intragroup medium in the H II regions to the Northwest of galaxy B, in sharp contrast to HCG 7 where the star-formation associated with each galaxy was self-contained. In the context of the evolutionary sequence we proposed in Konstantopoulos et al. (2010), it occupies a stage further along than HCG 7. It has begun building an IGM, as testified by some amount of intra-group light, but has yet to build up a large elliptical fraction. Its classification as a relatively unevolved group (J07) is in accord with standard diagnostics such as its velocity dispersion of ~ 335 km s^{-1} and lack of diffuse, extended X-ray emission.

Through the use of SDSS data, we associated five dwarf galaxies to HCG 59 for the first time. Their inclusion updated the velocity dispersion and dynamical mass of the group and changed its J07 evolutionary type to an evolved group of Type III (originally Type II, or intermediate). The star-forming nature of these dwarfs, their radial velocities, and distances from the group core seem to suggest that some may be infalling for the first time. The noted relation between morphological type and barycentric distance follows the one observed in the Local Group and may be considered – conversely – as an indication of the 'young' dynamical state of HCG 59. The above information highlights the importance of studying the dwarf galaxy contingent of compact groups.

Star formation is proceeding at a regular pace in this CG, certainly at a rate consistent with the morphologies of the member galaxies. The regularity of star cluster complexes agrees with this image. The star cluster population does not show evidence of major, gas-rich, interactions in the past $\sim$ Gyr and the IR SEDs are generally as expected. One exception to this rule is galaxy D. Given its large size, the morphological regularity of its neighbors, and the lack of evidence of recent interactions, it is not clear why it has such an irregular structure and why it is forming stars at the rate that it is.

Where the information is unclear for galaxy D, B is evidently in the midst of at least one dynamical process. This probably started more than a Gyr ago given the lack of tidal features such as shells and tails commonly observed in such events in the optical (Schweizer & Seitzer 1998; Hibbard et al. 2001; Mullan et al. 2011). It is likely physically associated with an arc of star formation that seemingly connects it to dwarf galaxy I (the arc that hosts the discovered extragalactic H II regions), and 59B lies at one end of a low surface brightness bridge of stellar material, which might physically connect it with A. We found this feature to be no older than ~ 1 Gyr by age-dating its stellar population. Perhaps most intriguingly, the globular cluster population of B is anomalously large, with significantly more globular cluster candidates than A, despite its lower stellar mass. The origin of this discrepancy is unclear, but hints at an additional event in the more distant past.

In one sense, this group is typical of early or intermediate-stage HCGs. There are plenty of dynamical processes at play, however they are all proceeding at a low level and centered around one or two objects. Galaxy B is at the focus of all such processes that our diagnostics can reach, like galaxy B in HCG 7 (also an early-type galaxy). In addition, both these groups may feature an active nucleus host galaxy (the dominant galaxy A in both groups, albeit the detection is not certain in HCG 7).

We find the presence of a low-luminosity AGN in A to be likely given the spatial coincidence of the galaxy centroid with a $\sim 10^{40}$ erg s^{-1} X-ray point source. The inferred SFR from the IR+UV luminosity is not supported given the lack of young star clusters, and therefore likely is overestimated because of significant AGN contamination. If the A-B bridge constitutes a physical connection between the two galaxies, a causal connection between the interaction and the AGN is possible. In this case, we can constrain the timescale since the

onset to no more than one Gyr.

In the introduction, we discussed HCGs as a potentially special environment in terms of galaxy evolution. The apparent duality of 'modes' in which HCG galaxies are found – either star-forming or quiescent – and the evident lack of an intermediate stage population are in accord with the mid-IR color-space 'gap' discussed in our previous work (Johnson et al. 2007; Tzanavaris et al. 2010; Walker et al. 2010). The impact of the group environment will be the topic of the next paper in this series. There we will treat HCGs 16, 22 and 42 with a goal of understanding the evolutionary processes at play in compact groups and relating their galaxies to those found at other levels of galaxy clustering.

Acknowledgements

REFERENCES

Arnaud, K. A. 1996, in Astronomical Society of the Pacific Conference Series, Vol. 101, Astronomical Data Analysis Software and Systems V, ed. G. H. Jacoby & J. Barnes, 17–+

Ashman, K. M., Bird, C. M., & Zepf, S. E. 1994, AJ, 108, 2348

Ashman, K. M., & Zepf, S. E. 1998, Globular Cluster Systems (Cambridge University Press)

Baldwin, J. A., Phillips, M. M., & Terlevich, R. 1981, PASP, 93, 5

Barkhouse, W. A., West, M. J., & Bothun, G. D. 2001, ApJ, 562, 679

Bastian, N., Ercolano, B., Gieles, M., Rosolowsky, E., Scheepmaker, R. A., Gutermuth, R., & Efremov, Y. 2007, MNRAS, 379, 1302

Bastian, N., Trancho, G., Konstantopoulos, I. S., & Miller, B. W. 2009, ApJ, 701, 607

Bell, E. F., Wolf, C., Meisenheimer, K., Rix, H., Borch, A., Dye, S., Kleinheinrich, M., Wisotzki, L., & McIntosh, D. H. 2004, ApJ, 608, 752

Belokurov, V., Zucker, D. B., Evans, N. W., Gilmore, G., Vidrih, S., Bramich, D. M., Newberg, H. J., Wyse, R. F. G., Irwin, M. J., Fellhauer, M., Hewett, P. C., Walton, N. A., Wilkinson, M. I., Cole, N., Yanny, B., Rockosi, C. M., Beers, T. C., Bell, E. F., Brinkmann, J., Ivezić, Ž., & Lupton, R. 2006, ApJ, 642, L137

Binggeli, B., Tammann, G. A., & Sandage, A. 1987, AJ, 94, 251

Bressert, E., Bastian, N., Gutermuth, R., Megeath, S. T., Allen, L., Evans, II, N. J., Rebull, L. M., Hatchell, J., Johnstone, D., Bourke, T. L., Cieza, L. A., Harvey, P. M., Merin, B.,

Ray, T. P., & Tothill, N. F. H. 2010, MNRAS, 409, L54

Broos, P. S., Townsley, L. K., Feigelson, E. D., Getman, K. V., Bauer, F. E., & Garmire, G. P. 2010, ApJ, 714, 1582

Bruzual, G., & Charlot, S. 2003, MNRAS, 344, 1000

Cappelluti, N., Hasinger, G., Brusa, M., Comastri, A., Zamorani, G., Böhringer, H., Brunner, H., Civano, F., Finoguenov, A., Fiore, F., Gilli, R., Griffiths, R. E., Mainieri, V., Matute, I., Miyaji, T., & Silverman, J. 2007, ApJS, 172, 341

Cardelli, J. A., Clayton, G. C., & Mathis, J. S. 1989, ApJ, 345, 245

Chandar, R., Whitmore, B., & Lee, M. G. 2004, ApJ, 611, 220

Chou, M., Majewski, S. R., Cunha, K., Smith, V. V., Patterson, R. J., Martínez-Delgado, D., Law, D. R., Crane, J. D., Muñoz, R. R., Garcia López, R., Geisler, D., & Skrutskie, M. F. 2007, ApJ, 670, 346

Correnti, M., Bellazzini, M., Ibata, R. A., Ferraro, F. R., & Varghese, A. 2010, ApJ, 721, 329

Cox, ed. 2000, Allen's astrophysical quantities (AIP Press)

Da Rocha, C., & Mendes de Oliveira, C. 2005, MNRAS, 364, 1069

Da Rocha, C., Mendes de Oliveira, C., Bolte, M., Ziegler, B. L., & Puzia, T. H. 2002, AJ, 123, 690

Da Rocha, C., Ziegler, B. L., & Mendes de Oliveira, C. 2008, MNRAS, 388, 1433

de Vaucouleurs, G., de Vaucouleurs, A., Corwin, Jr., H. G., Buta, R. J., Paturel, G., & Fouque, P. 1991, Third Reference Catalogue of Bright Galaxies (Volume 1-3, XII, 2069 pp. 7 figs.. Springer-Verlag Berlin Heidelberg New York)

Efremov, Y. N., Ivanov, G. R., & Nikolov, N. S. 1986, in IAU Symposium, Vol. 116, Luminous Stars and Associations in Galaxies, ed. C. W. H. de Loore, A. J. Willis, & P. Laskarides, 389–+

Elmegreen, B. G., Elmegreen, D. M., Salzer, J. J., & Mann, H. 1996, ApJ, 467, 579

Elmegreen, D. M., Elmegreen, B. G., Lang, C., & Stephens, C. 1994, ApJ, 425, 57

Elmegreen, D. M., Elmegreen, B. G., Marcus, M. T., Shahinyan, K., Yau, A., & Petersen, M. 2009, ApJ, 701, 306

Elvis, M., Wilkes, B. J., McDowell, J. C., Green, R. F., Bechtold, J., Willner, S. P., Oey, M. S., Polomski, E., & Cutri, R. 1994, ApJS, 95, 1

Evans, I. N., Primini, F. A., Glotfelty, K. J., Anderson, C. S., Bonaventura, N. R., Chen, J. C., Davis, J. E., Doe, S. M., Evans, J. D., Fabbiano, G., Galle, E. C., Gibbs, D. G., Grier, J. D., Hain, R. M., Hall, D. M., Harbo, P. N., (Helen He, X., Houck, J. C., Karovska, M., Kashyap, V. L., Lauer, J., McCollough, M. L., McDowell, J. C., Miller, J. B., Mitschang, A. W., Morgan, D. L., Mossman, A. E., Nichols, J. S., Nowak, M. A., Plummer, D. A., Refsdal, B. L., Rots, A. H., Siemiginowska, A., Sundheim, B. A., Tibbetts, M. S., Van Stone, D. W., Winkelman, S. L., & Zografou, P. 2010, ApJS, 189, 37

Falco, E. E., Kurtz, M. J., Geller, M. J., Huchra, J. P., Peters, J., Berlind, P., Mink, D. J., Tokarz, S. P., & Elwell, B. 1999, PASP, 111, 438

Freeman, P. E., Kashyap, V., Rosner, R., & Lamb, D. Q. 2002, ApJS, 138, 185

Fruchter, A., & Sosey, M. 2009 (STScI)

Fujita, Y., & Goto, T. 2004, PASJ, 56, 621

Gallagher, S. C., Durrell, P. R., Elmegreen, D. M., Chandar, R., English, J., Charlton, J. C., Gronwall, C., Young, J., Tzanavaris, P., Johnson, K. E., de Oliveira, C. M., Whitmore, B., Hornschemeier, A. E., Maybhate, A., , & Zabludoff, A. 2010, The Astronomical Journal, 139, 545

Gallagher, S. C., Johnson, K. E., Hornschemeier, A. E., Charlton, J. C., & Hibbard, J. E. 2008, ApJ, 673, 730

Gallagher, S. C., Richards, G. T., Hall, P. B., Brandt, W. N., Schneider, D. P., & Vanden Berk, D. E. 2005, AJ, 129, 567

Gehrels, N. 1986, ApJ, 303, 336

Grebel, E. K. 1999, in IAU Symposium, Vol. 192, The Stellar Content of Local Group Galaxies, ed. P. Whitelock & R. Cannon, 17–+

Harris, W. E. 1996, AJ, 112, 1487

Harris, W. E. 2001, in Saas-Fee Advanced Course 28: Star Clusters, ed. L. Labhardt & B. Binggeli, 223–+

Haynes, M. P., & Giovanelli, R. 1984, AJ, 89, 758

Hibbard, J. E., van Gorkom, J. H., Rupen, M. P., & Schiminovich, D. 2001, in Astronomical Society of the Pacific Conference Series, Vol. 240, Gas and Galaxy Evolution, ed. J. E. Hibbard, M. Rupen, & J. H. van Gorkom, 657–+

Hickson, P. 1982, ApJ, 255, 382

Hickson, P., Kindl, E., & Auman, J. R. 1989, ApJS, 70, 687

Hickson, P., Mendes de Oliveira, C., Huchra, J. P., & Palumbo, G. G. 1992, ApJ, 399, 353

Ho, L. C., Feigelson, E. D., Townsley, L. K., Sambruna, R. M., Garmire, G. P., Brandt, W. N., Filippenko, A. V., Griffiths, R. E., Ptak, A. F., & Sargent, W. L. W. 2001, ApJ, 549, L51

Johnson, K. E., Hibbard, J. E., Gallagher, S. C., Charlton, J. C., Hornschemeier, A. E., Jarrett, T. H., & Reines, A. E. 2007, AJ, 134, 1522

Jones, L. R., Ponman, T. J., Horton, A., Babul, A., Ebeling, H., & Burke, D. J. 2003, MNRAS, 343, 627

Kalberla, P. M. W., Burton, W. B., Hartmann, D., Arnal, E. M., Bajaja, E., Morras, R., & Pöppel, W. G. L. 2005, A&A, 440, 775

Kewley, L. J., Groves, B., Kauffmann, G., & Heckman, T. 2006, MNRAS, 372, 961

Konstantopoulos, I. S. 2009, ArXiv e-prints

Konstantopoulos, I. S., Bastian, N., Smith, L. J., Trancho, G., Westmoquette, M. S., & Gallagher, III, J. S. 2008, ApJ, 674, 846

Konstantopoulos, I. S., Bastian, N., Smith, L. J., Westmoquette, M. S., Trancho, G., & Gallagher, J. S. 2009, ApJ, 701, 1015

Konstantopoulos, I. S., Gallagher, S. C., Fedotov, K., Durrell, P. R., Heiderman, A., Elmegreen, D. M., Charlton, J. C., Hibbard, J. E., Tzanavaris, P., Chandar, R., Johnson, K. E., Maybhate, A., Zabludoff, A. E., Gronwall, C., Szathmary, D., Hornschemeier, A. E., English, J., Whitmore, B., Mendes de Oliveira, C., & Mulchaey, J. S. 2010, ApJ, 723, 197

Lada, C. J., & Lada, E. A. 2003, ARA&A, 41, 57

Leitherer, C., Schaerer, D., Goldader, J. D., González Delgado, R. M., Robert, C., Kune, D. F., de Mello, D. F., Devost, D., & Heckman, T. M. 1999, ApJS, 123, 3

Majewski, S. R., Skrutskie, M. F., Weinberg, M. D., & Ostheimer, J. C. 2003, ApJ, 599, 1082

Marigo, P., Girardi, L., Bressan, A., Groenewegen, M. A. T., Silva, L., & Granato, G. L. 2008, A&A, 482, 883

Martínez, M. A., Del Olmo, A., Coziol, R., & Perea, J. 2010, AJ, 139, 1199

Mulchaey, J. S., & Zabludoff, A. I. 1998, ApJ, 496, 73

Mullan, B., Konstantopoulos, I. S., Kepley, A. A., Lee, K. H., Charlton, J. C., Knierman, K., Bastian, N., Chandar, R., Durrell, P. R., Elmegreen, D., English, J., Gallagher, S. C., Gronwall, C., Hibbard, J. E., Hunsberger, S., Johnson, K. E., Maybhate, A., Palma, C., Trancho, G., & Vacca, W. D. 2011, ArXiv e-prints

Muratov, A. L., & Gnedin, O. Y. 2010, ArXiv e-prints

Newberg, H. J., Yanny, B., Cole, N., Beers, T. C., Re Fiorentin, P., Schneider, D. P., & Wilhelm, R. 2007, ApJ, 668, 221

Niederste-Ostholt, M., Belokurov, V., Evans, N. W., & Peñarrubia, J. 2010, ApJ, 712, 516

Palma, C., Zonak, S. G., Hunsberger, S. D., Charlton, J. C., Gallagher, S. C., Durrell, P. R., & English, J. 2002, AJ, 124, 2425

Peng, C. Y., Ho, L. C., Impey, C. D., & Rix, H.-W. 2010a, AJ, 139, 2097

36

—. 2010b, AJ, 139, 2097

Pirzkal, N., Sahu, K. C., Burgasser, A., Moustakas, L. A., Xu, C., Malhotra, S., Rhoads, J. E., Koekemoer, A. M., Nelan, E. P., Windhorst, R. A., Panagia, N., Gronwall, C., Pasquali, A., & Walsh, J. R. 2005, ApJ, 622, 319

Popescu, B., & Hanson, M. M. 2010, ApJ, 724, 296

Rejkuba, M., Greggio, L., Harris, W. E., Harris, G. L. H., & Peng, E. W. 2005, ApJ, 631, 262

Rhode, K. L., Zepf, S. E., Kundu, A., & Larner, A. N. 2007, AJ, 134, 1403

Robin, A. C., Reylé, C., Derrière, S., & Picaud, S. 2003, A&A, 409, 523

Rubin, V. C., Hunter, D. A., & Ford, Jr., W. K. 1990, ApJ, 365, 86

Rudick, C. S., Mihos, J. C., & McBride, C. 2006, ApJ, 648, 936

Scheepmaker, R. A., Haas, M. R., Gieles, M., Bastian, N., Larsen, S. S., & Lamers, H. J. G. L. M. 2007, A&A, 469, 925

Schlegel, D. J., Finkbeiner, D. P., & Davis, M. 1998, ApJ, 500, 525

Schweizer, F., & Seitzer, P. 1998, AJ, 116, 2206

Sérsic, J. L. 1968, Atlas de galaxias australes (Observatorio Astronomico)

Silva, L., Granato, G. L., Bressan, A., & Danese, L. 1998, ApJ, 509, 103

Silva-Villa, E., & Larsen, S. 2011, ArXiv e-prints

Sirianni, M., Jee, M. J., Benítez, N., Blakeslee, J. P., Martel, A. R., Meurer, G., Clampin, M., De Marchi, G., Ford, H. C., Gilliland, R., Hartig, G. F., Illingworth, G. D., Mack, J., & McCann, W. J. 2005, PASP, 117, 1049

Skrutskie, M. F., Cutri, R. M., Stiening, R., Weinberg, M. D., Schneider, S., Carpenter, J. M., Beichman, C., Capps, R., Chester, T., Elias, J., Huchra, J., Liebert, J., Lonsdale, C., Monet, D. G., Price, S., Seitzer, P., Jarrett, T., Kirkpatrick, J. D., Gizis, J. E., Howard, E., Evans,

T., Fowler, J., Fullmer, L., Hurt, R., Light, R., Kopan, E. L., Marsh, K. A., McCallon, H. L., Tam, R., Van Dyk, S., & Wheelock, S. 2006, AJ, 131, 1163

Smith, L. J., Bastian, N., Konstantopoulos, I. S., Gallagher, III, J. S., Gieles, M., de Grijs, R., Larsen, S. S., O'Connell, R. W., & Westmoquette, M. S. 2007, ApJL, 667, L145

Tago, E., Einasto, J., Saar, E., Tempel, E., Einasto, M., Vennik, J., & Müller, V. 2008, A&A, 479, 927

The, L. S., & White, S. D. M. 1986, AJ, 92, 1248

Trancho, G., Bastian, N., Miller, B. W., & Schweizer, F. 2007, ApJ, 664, 284

Tzanavaris, P., Hornschemeier, A. E., Gallagher, S. C., Johnson, K. E., Gronwall, C., Immler, S., Reines, A. E., Hoversten, E., & Charlton, J. C. 2010, ApJ, 716, 556

Verdes-Montenegro, L., Yun, M. S., Perea, J., del Olmo, A., & Ho, P. T. P. 1998, ApJ, 497, 89

Verdes-Montenegro, L., Yun, M. S., Williams, B. A., Huchtmeier, W. K., Del Olmo, A., & Perea, J. 2001, A&A, 377, 812

Walker, L. M., Johnson, K. E., Gallagher, S. C., Hibbard, J. E., Hornschemeier, A. E., Tzanavaris, P., Charlton, J. C., & Jarrett, T. H. 2010, AJ, 140, 1254

White, P. M., Bothun, G., Guerrero, M. A., West, M. J., & Barkhouse, W. A. 2003, ApJ, 585, 739

Xue, Y. Q., Luo, B., Brandt, W. N., Bauer, F. E., Lehmer, B. D., Broos, P. S., Schneider, D. P., Alexander, D. M., Brusa, M., Comastri, A., Fabian, A. C., Gilli, R., Hasinger, G., Hornschemeier, A. E., Koekemoer, A., Liu, T., Mainieri, V., Paolillo, M., Rafferty, D. A., Rosati, P., Shemmer, O., Silverman, J. D., Smail, I., Tozzi, P., & Vignali, C. 2011, ApJS, 195, 10

Yanny, B., Newberg, H. J., Johnson, J. A., Lee, Y. S., Beers, T. C., Bizyaev, D., Brewington, H., Fiorentin, P. R., Harding, P., Malanushenko, E., Malanushenko, V., Oravetz, D., Pan, K., Simmons, A., & Snedden, S. 2009, ApJ, 700, 1282

York, D. G., Adelman, J., Anderson, Jr., J. E., Anderson, S. F., Annis, J., Bahcall, N. A., Bakken, J. A., Barkhouser, R., Bastian, S., Berman, E., Boroski, W. N., Bracker, S., Briegel, C., Briggs, J. W., Brinkmann, J., Brunner, R., Burles, S., Carey, L., Carr, M. A., Castander, F. J., Chen, B., Colestock, P. L., Connolly, A. J., Crocker, J. H., Csabai, I., Czarapata, P. C., Davis, J. E., Doi, M., Dombeck, T., Eisenstein, D., Ellman, N., Elms, B. R., Evans, M. L., Fan, X., Federwitz, G. R., Fiscelli, L., Friedman, S., Frieman, J. A., Fukugita, M., Gillespie, B., Gunn, J. E., Gurbani, V. K., de Haas, E., Haldeman, M., Harris, F. H., Hayes, J., Heckman, T. M., Hennessy, G. S., Hindsley, R. B., Holm, S., Holmgren, D. J., Huang, C., Hull, C., Husby, D., Ichikawa, S., Ichikawa, T., Ivezić, Ž., Kent, S., Kim, R. S. J., Kinney, E., Klaene, M., Kleinman, A. N., Kleinman, S., Knapp, G. R., Korienek, J., Kron, R. G., Kunszt, P. Z., Lamb, D. Q., Lee, B., Leger, R. F., Limmongkol, S., Lindenmeyer, C., Long, D. C., Loomis, C., Loveday, J., Lucinio, R., Lupton, R. H., MacKinnon, B., Mannery, E. J., Mantsch, P. M., Margon, B., McGehee, P., McKay, T. A., Meiksin, A., Merelli, A., Monet, D. G., Munn, J. A., Narayanan, V. K., Nash, T., Neilsen, E., Neswold, R., Newberg, H. J., Nichol, R. C., Nicinski, T., Nonino, M., Okada, N., Okamura, S., Ostriker, J. P., Owen, R., Pauls, A. G., Peoples, J., Peterson, R. L., Petravick, D., Pier, J. R., Pope, A., Pordes, R., Prosapio, A., Rechenmacher, R., Quinn, T. R., Richards, G. T., Richmond, M. W., Rivetta, C. H., Rockosi, C. M., Ruthmansdorfer, K., Sandford, D., Schlegel, D. J., Schneider, D. P., Sekiguchi, M., Sergey, G., Shimasaku, K., Siegmund, W. A., Smee, S., Smith, J. A., Snedden, S., Stone, R., Stoughton, C., Strauss, M. A., Stubbs, C., SubbaRao, M., Szalay, A. S., Szapudi, I., Szokoly, G. P., Thakar, A. R., Tremonti, C., Tucker, D. L., Uomoto, A., Vanden Berk, D., Vogeley, M. S., Waddell, P., Wang, S., Watanabe, M., Weinberg, D. H., Yanny, B., & Yasuda, N. 2000, AJ, 120, 1579

Zabludoff, A. I., & Mulchaey, J. S. 2000, ApJ, 539, 136